

Tachyonic and Plasma Instabilities of η -Pairing States Coupled to Electromagnetic Fields

Naoto Tsuji,^{1,2} Masaya Nakagawa,¹ and Masahito Ueda^{1,2,3}

¹*Department of Physics, University of Tokyo, Hongo, Tokyo 113-0033, Japan*

²*RIKEN Center for Emergent Matter Science (CEMS), Wako 351-0198, Japan*

³*Institute for Physics of Intelligence, University of Tokyo, Hongo, Tokyo 113-0033, Japan*

(Dated: February 1, 2022)

Cooper pairs featuring a nonzero center-of-mass crystal momentum $\mathbf{Q} = (\pi, \pi, \dots)$ and an off-diagonal long-range order (η -pairing states) constitute exact eigenstates of a Hubbard model [C. N. Yang, Phys. Rev. Lett. **63**, 2144 (1989)]. Here we show that the η -pairing states are rendered dynamically unstable via coupling to dynamical electromagnetic fields. The instability is caused by “tachyonic” electromagnetic fields and unstable plasma modes for attractive and repulsive interactions, respectively. The typical time scale of the growth of the instability is of the order of femtoseconds for electron systems in solids, which places a strict bound on the lifetime of the η -pairing states. The decay of the η -pairing states leads to enhanced light emission with frequencies shifted from the Hubbard interaction strength for the repulsive case and unattenuated electromagnetic penetration for the attractive case.

Introduction.— A search for long-lived non-thermal excited states that support macroscopic long-range order is a modern challenge in nonequilibrium condensed matter physics. If such a state exists, a rich variety of possibilities arises that could extend the landscape of long-range order in solid-state materials. In fact, there have been a number of experimental reports on the possible existence of nonequilibrium long-range order, including light-induced [1–7] or quench-induced [8] superconductivity (see also [9, 10]), photoinduced ferromagnetism [11, 12] and charge density waves [13–15]. While the experimental progress is underway, the theoretical understanding is yet to be made. A major challenge is that an analysis of excited states in quantum many-body systems often requires approximations that render the conclusion on the existence of such a state highly nontrivial.

A very exception to this situation is the η -pairing states, which are known to be exact eigenstates of a Hubbard model as revealed by C. N. Yang [16]. The η -pairing states exhibit a number of remarkable features. In particular, they have an off-diagonal long-range order (ODLRO) in arbitrary dimensions even though their eigenenergies lie much higher than the ground state. This is to be contrasted with finite-temperature thermal states, which cannot show ODLROs in one and two dimensions due to the Mermin-Wagner theorem. The non-thermal nature of the η -pairing states has also been discussed recently in the context of quantum many-body scars [17–19].

The presence of such a non-thermal state suggests that the η -pairing states with an ODLRO (and hence superconductivity) might be realized in nonequilibrium situations. Recent theoretical studies have demonstrated that this is indeed possible in several different setups, including periodic [20–23] and pulsed [24–27] electric-field drives, dissipation engineering [28, 29], spin-dependent dephasing [30, 31], and spontaneous light emission [32].

These mechanisms will work for the Hubbard model with or without coupling to an external bath, which may be realized in electrically neutral ultracold atoms trapped in an optical lattice.

In view of applications to real materials, one cannot ignore the coupling of electrons to *dynamical electromagnetic fields*, since electrons have electric charges. This point is crucial for the stability of the η -pairing states supported by the long lifetime of doublons. If doublons decay into single particles or lose their momenta, they induce local electric currents due to charge transfer, which then generate dynamical electromagnetic fields. The effect of the latter feedbacks to electrons, and causes collective modes of electromagnetic fields, which accelerate the relaxation of doublons. Such a dynamical instability deserves careful scrutiny in view of growing attention in nonequilibrium superconductivity.

In this Letter, we study the dynamics of the η -pairing states in the Hubbard model coupled to dynamical electromagnetic fields. Our approach is based on the exact solution of the electromagnetic response function (or the Meissner kernel) $K^{\mu\nu}(\mathbf{q}, \omega)$ with full momentum (\mathbf{q}) and frequency (ω) dependences. In contrast, previous studies have focused on the static and uniform limit (i.e., $\mathbf{q} = \omega = 0$) [25, 33, 34]. As we will see, the momentum and frequency dependences play a pivotal role in dynamical instabilities of η -pairing states. Combining the obtained results with the Maxwell equations, we rigorously prove the existence of the “tachyonic” and plasma instabilities for attractively and repulsively interacting systems, respectively. The time scale of the growth of the instability is surprisingly short, being of the order of femtoseconds or even shorter than that for ordinary materials. This puts a severe constraint on the lifetime of the η -pairing states in electron systems. Finally, we discuss that the decay of the η -pairing states leads to intense light emission with frequencies shifted from the

interaction strength in the repulsive case, and unattenuated penetration of electromagnetic fields in the attractive case.

η pairing in the Hubbard model.— We consider the Hubbard model on a d -dimensional cubic lattice subject to the periodic boundary condition with the Hamiltonian,

$$H = -t_h \sum_{\langle ij \rangle, \sigma} (c_{i\sigma}^\dagger c_{j\sigma} + \text{H.c.}) + U \sum_i n_{i\uparrow} n_{i\downarrow} - \frac{U}{2} \sum_{i\sigma} n_{i\sigma}, \quad (1)$$

where t_h (> 0) is the hopping amplitude, $c_{i\sigma}^\dagger$ is a creation operator of an electron at site i with spin $\sigma = \uparrow, \downarrow$, $\langle ij \rangle$ represents a pair of nearest-neighbor lattice sites, U is the on-site interaction strength, and $n_{i\sigma} = c_{i\sigma}^\dagger c_{i\sigma}$ is the particle-number operator. Since we fix the total number of electrons throughout this Letter, the last term in Eq. (1) is a constant. We set the lattice constant $a = 1$ and the Planck constant $\hbar = 1$ unless otherwise noted.

The Hubbard model (1) has the spin $\text{SU}(2)$ symmetry together with the “hidden” η $\text{SU}(2)$ symmetry, which altogether form the symmetry of $\text{SU}(2) \times \text{SU}(2)/\mathbb{Z}_2 \simeq \text{SO}(4)$ [35]. The existence of η -pairing states as the exact eigenstates of the Hubbard model essentially relies on this fact. To see the η symmetry, we define the η operators, $\eta^+ := \sum_j e^{i\mathbf{Q} \cdot \mathbf{R}_j} c_{j\uparrow}^\dagger c_{j\downarrow}^\dagger$, $\eta^- := (\eta^+)^\dagger$, and $\eta^z := \frac{1}{2} \sum_j (n_{j\uparrow} + n_{j\downarrow} - 1)$, where $\mathbf{Q} = (\pi, \pi, \dots)$ is the momentum at the Brillouin-zone corner, and \mathbf{R}_j is the position vector of lattice site j . The η operators satisfy the ordinary $\text{su}(2)$ algebra, i.e., $[\eta^+, \eta^-] = 2\eta^z$ and $[\eta^z, \eta^\pm] = \pm\eta^\pm$. From direct calculations, one can confirm that they all commute with the Hamiltonian (1): $[H, \eta^\alpha] = 0$ ($\alpha = \pm, z$).

Using the η operators, one can construct Yang’s η -pairing states. The simplest one is

$$|\psi_N\rangle = \frac{1}{\sqrt{\mathcal{N}_N}} (\eta^+)^{\frac{N}{2}} |0\rangle, \quad (2)$$

where N is the number of electrons which is assumed to be an even integer, \mathcal{N}_N is the normalization constant (such that $\langle \psi_N | \psi_N \rangle = 1$), and $|0\rangle$ is the vacuum state. The η -pairing state $|\psi_N\rangle$ consists of $\frac{N}{2}$ doublons having momentum \mathbf{Q} . Since η^+ commutes with H (1), $|\psi_N\rangle$ (2) is indeed the exact eigenstate of H with the eigenenergy $E_N = 0$ in arbitrary dimensions. The state $|\psi_N\rangle$ (2) has the ODLRO $\frac{1}{2} \langle \psi_N | (c_{i\uparrow}^\dagger c_{i\downarrow}^\dagger c_{j\downarrow} c_{j\uparrow} + \text{H.c.}) | \psi_N \rangle = e^{i\mathbf{Q} \cdot (\mathbf{R}_i - \mathbf{R}_j)} C_{M,N}$ [16] ($C_{M,N} := \frac{\frac{N}{2}(M - \frac{N}{2})}{M(M-1)}$ and M is the number of lattice sites), which saturates the upper bound of ODLRO [32, 36]. Physically, $|\psi_N\rangle$ (2) corresponds to the condensate of spin-singlet Cooper pairs with the center-of-mass momentum \mathbf{Q} .

Electromagnetic response of η -pairing states.— We study the electromagnetic response of the η -pairing state $|\psi_N\rangle$ (2) within the linear-response regime. We focus on the three-dimensional case ($d = 3$). However, most of

the results in the present Letter can straightforwardly be extended to other dimensions. The response of the current against an external electromagnetic field with momentum \mathbf{q} and frequency ω is given by $j^\mu(\mathbf{q}, \omega) = -K^{\mu\nu}(\mathbf{q}, \omega) A_\nu(\mathbf{q}, \omega)$ ($\mu, \nu = x, y, z$), where $K^{\mu\nu}(\mathbf{q}, \omega)$ is the Meissner kernel [37] and $A_\nu(\mathbf{q}, \omega)$ is the vector potential.

In general, the kernel $K^{\mu\nu}(\mathbf{q}, \omega)$ consists of the paramagnetic and diamagnetic components [37]. In the case of η -pairing states, the diamagnetic component vanishes exactly, since it is proportional to the kinetic energy [38], which vanishes for the η -pairing states. This is in stark contrast to ordinary superconductors, in which perfect diamagnetism arises from the diamagnetic component of the Meissner kernel. In the η -pairing states, the paramagnetic component takes over the role of the diamagnetic one in ordinary superconductors.

The paramagnetic component is given by the Kubo formula,

$$K_{\text{para}}^{\mu\nu}(\mathbf{R}_j, t) = -i\theta(t) \langle \psi_N | [J^\mu(\mathbf{R}_j, t), J^\nu(0, 0)] | \psi_N \rangle, \quad (3)$$

where $\theta(t)$ is the unit-step function ($\theta(t) = 1$ for $t \geq 0$ and $\theta(t) = 0$ otherwise), and $J^\mu(\mathbf{R}_j, t)$ is the local current operator at site j and time t in the Heisenberg picture. The local current $J^\mu(\mathbf{R}_j, 0) = J^\mu(\mathbf{R}_j)$ is expressed explicitly as $J^\mu(\mathbf{R}_j) = -iet_h \sum_\sigma (c_{j+\mu, \sigma}^\dagger c_{j\sigma} - c_{j\sigma}^\dagger c_{j+\mu, \sigma})$, where e is the electric charge, and $j + \mu$ represents the nearest-neighbor site of j in the μ direction.

We can evaluate Eq. (3) exactly for arbitrary \mathbf{R}_j and t using the following algebraic relations: $[J^\mu(\mathbf{R}_j), \eta^\pm] = \pm 2J_\eta^{\mu\pm}(\mathbf{R}_j)$, $[J_\eta^{\mu\pm}(\mathbf{R}_j), \eta^\pm] = 0$, and $[J_\eta^{\mu\pm}(\mathbf{R}_j), \eta^\mp] = \pm J^\mu(\mathbf{R}_j)$. They allow us to reduce the N -particle correlation function (3) to that of the vacuum state [39],

$$K_{\text{para}}^{\mu\nu}(\mathbf{R}_j, t) = -4i\theta(t) C_{M,N} [\langle 0 | J_\eta^{\mu-}(\mathbf{R}_j, t) J_\eta^{\nu+}(0, 0) | 0 \rangle - \langle 0 | J_\eta^{\nu-}(0, 0) J_\eta^{\mu+}(\mathbf{R}_j, t) | 0 \rangle]. \quad (4)$$

In this way, the N -particle problem reduces to the two-particle problem, which is exactly solvable [40].

We further decompose the kernel into the transverse and longitudinal components. Without loss of generality, we assume that the momentum \mathbf{q} of the vector potential points in the z direction. The transverse component is defined as $K^\perp(\mathbf{q}, \omega) := K^{\mu\mu}(\mathbf{q}, \omega)$ ($\mu = x, y$), while the longitudinal one is $K^\parallel(\mathbf{q}, \omega) := K^{zz}(\mathbf{q}, \omega)$. The kernel does not have the off-diagonal components ($K^{\mu\nu}(\mathbf{q}, \omega) = 0$ for $\mu \neq \nu$) [39]. In the two-particle dynamics involved in Eq. (4), the center-of-mass momentum and the relative coordinates in the x and y directions of the two particles are conserved. In addition, for the transverse components the two particles never sit at the same site, making the dynamics effectively noninteracting. These observations lead us to an analytical solution

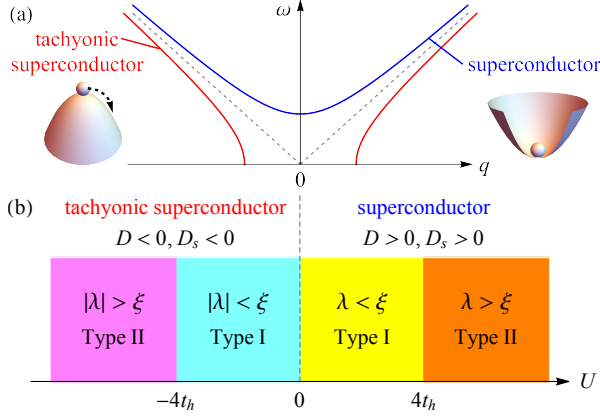


FIG. 1. (a) Schematic dispersion of electromagnetic fields and their effective potentials (3D images) for ordinary superconductors and tachyonic superconductors. The dashed lines show the dispersion relation of electromagnetic fields in the vacuum. (b) Phase diagram of the η -pairing states in the Hubbard model.

for the transverse component [39],

$$K^\perp(\mathbf{q}, \omega) = -8ie^2 t_h C_{M,N} \left[f_q\left(\frac{\omega+U}{t_h}\right) - f_q\left(\frac{\omega-U}{t_h}\right) \right],$$

$$f_q(x) := \begin{cases} \frac{i \operatorname{sgn}(x)}{\sqrt{x^2 - 16 \sin^2 \frac{q}{2}}} & \text{for } |x| > 4 \sin \frac{q}{2}; \\ \frac{1}{\sqrt{16 \sin^2 \frac{q}{2} - x^2}} & \text{for } |x| < 4 \sin \frac{q}{2}, \end{cases} \quad (5)$$

where q (> 0) is the z component of \mathbf{q} . The longitudinal component does not have such a compact expression, but can be evaluated exactly in a similar manner [39].

The exact solution (5) for the electromagnetic response function reveals a number of important properties of the η -pairing states. By taking the limit $\lim_{\mathbf{q} \rightarrow 0} \lim_{\omega \rightarrow 0} K^\perp(\mathbf{q}, \omega) = \frac{16e^2 t_h^2}{U} C_{M,N} =: \frac{1}{\pi} D_s$, one can recover the Meissner weight or superfluid stiffness D_s in Refs. [33, 34]. By taking another limit $\lim_{\mathbf{q} \rightarrow 0} K^\perp(\mathbf{q}, \omega) =: -i\omega\sigma(\omega)$, one obtains the optical conductivity, $\sigma(\omega) = \frac{8ie^2 t_h^2 C_{M,N}}{\omega + i\delta} \left(\frac{1}{\omega + U + i\delta} - \frac{1}{\omega - U + i\delta} \right)$ (δ is a positive infinitesimal constant), the real part of which shows delta-function-like peaks at $\omega = 0$ and $\pm U$. If one split the optical conductivity into the singular part at $\omega = 0$ and the regular part as $\operatorname{Re} \sigma(\omega) = D\delta(\omega) + \sigma_{\text{reg}}(\omega)$, one obtains the Drude weight or charge stiffness $D = \frac{16\pi e^2 t_h^2}{U} C_{M,N}$ [25]. For the distinction between D and D_s , we refer to Ref. [41].

For $U > 0$, D_s becomes positive, where the electromagnetic field acquires a mass due to the Anderson-Higgs mechanism [42, 43] [$\omega^2 \simeq c^2 q^2 + m^2 c^4$ with c the speed of light and $m^2 \propto D_s > 0$, see Fig. 1(a)]. On the other hand, for $U < 0$, D_s takes a negative value, implying that the electromagnetic field has a negative squared mass [$m^2 \propto D_s < 0$, Fig. 1(a)]. Thus, the system is a “tachyonic” superconductor [44] [see the phase diagram in Fig. 1(b)], in which the vacuum of the electromagnetic

field lies at the local maximum of the effective potential $V_{\text{eff}}(\mathbf{A}) \propto m^2 \mathbf{A}^2$ [Fig. 1(a)]. The electromagnetic field in the tachyonic superconductor becomes unstable, and starts to grow exponentially in time. The repulsive case ($U > 0$) does not have such a tachyonic instability, but shows a different type of instability, as discussed below.

If we look at the electromagnetic response closer, we find that there is a *phase transition* at $U = \pm 4t_h$ [Fig. 1(b)]. This can be seen from the behavior of the Meissner kernel represented in real space $K^\perp(j, \omega = 0)$ [39], which asymptotically decays exponentially as $\sim \exp(-j/\xi)$ with $\xi = 1/\cosh^{-1}(U^2/8t_h^2 - 1)$ for $|U| > 4t_h$ [39]. Here ξ is Pippard’s coherence length [37], which diverges at $U_c = \pm 4t_h$ as $\xi \sim |U - U_c|^{-1/2}$. For $|U| < 4t_h$, the kernel shows a power-law decay as $\sim j^{-1/2}$ [39].

Let us compare the coherence length ξ with London’s penetration depth λ defined by $\frac{1}{\lambda^2} = \frac{\mu_0}{\pi} D_s$ (μ_0 is the vacuum permeability). For $U > 0$, we have $\lambda = \sqrt{\frac{U}{16\mu_0 e^2 t_h^2 C_{M,N}}}$, which grows smoothly as U increases. In the region of $0 < U < 4t_h$, the penetration depth is smaller than the coherence length ($\lambda < \xi$), and the system belongs to type-I superconductors (Fig. 1). For $U > 4t_h$, on the other hand, the relation becomes opposite ($\lambda > \xi$), and the system turns to a type-II superconductor (Fig. 1) [45]. In an analogous way, we call the region $-4t_h < U < 0$ ($U < -4t_h$) a type-I (type-II) tachyonic superconductor (Fig. 1). They have different magnetic properties (for details, see [39]).

Dynamical instability of η -pairing states.— Now, let us study the dynamics of electromagnetic fields coupled to the η -pairing states for $U > 0$. To this end, we consider the Maxwell equation in the Lorenz gauge, $-\frac{\omega^2}{c^2} \mathbf{A} + q^2 \mathbf{A} = \mu_0 \mathbf{j}$, combined with the response of the η -pairing states, $j^\mu = -K^{\mu\nu}(\mathbf{q}, \omega) A_\nu$. The equation of motion determines the energy dispersion of collective modes of electromagnetic fields coupled with the η -pairing states. We focus on the transverse mode, whose energy dispersion is given by

$$\frac{\omega^2}{c^2} - q^2 = \mu_0 K^\perp(\mathbf{q}, \omega). \quad (6)$$

At $\mathbf{q} = 0$, Eq. (6) becomes $\frac{\omega^2}{c^2} = -\frac{16e^2 t_h^2 C_{M,N} U}{\omega^2 - U^2}$, which has imaginary-frequency solutions when $U^3 < 64\mu_0 e^2 c^2 t_h^2 C_{M,N}$. If we input $t_h = 1$ [eV] and $a = 1$ [Å] for ordinary materials, the condition reads $U/t_h < 22.6 \cdot (\rho(1-\rho))^{1/3}$, where $\rho := (N/2)/M$ is the number of doublons per site ($0 \leq \rho \leq 1$). Surprisingly, the η -pairing states coupled to electromagnetic fields are dynamically unstable over a wide range of the parameter space against $\mathbf{q} = 0$ modes. More generally, we find that the η -pairing states are unstable for all the parameters if we take into account arbitrary \mathbf{q} modes.

In Fig. 2, we plot the numerical solutions of Eq. (6) for various parameters. In Figs. 2(a) ($U > 0$) and (b)

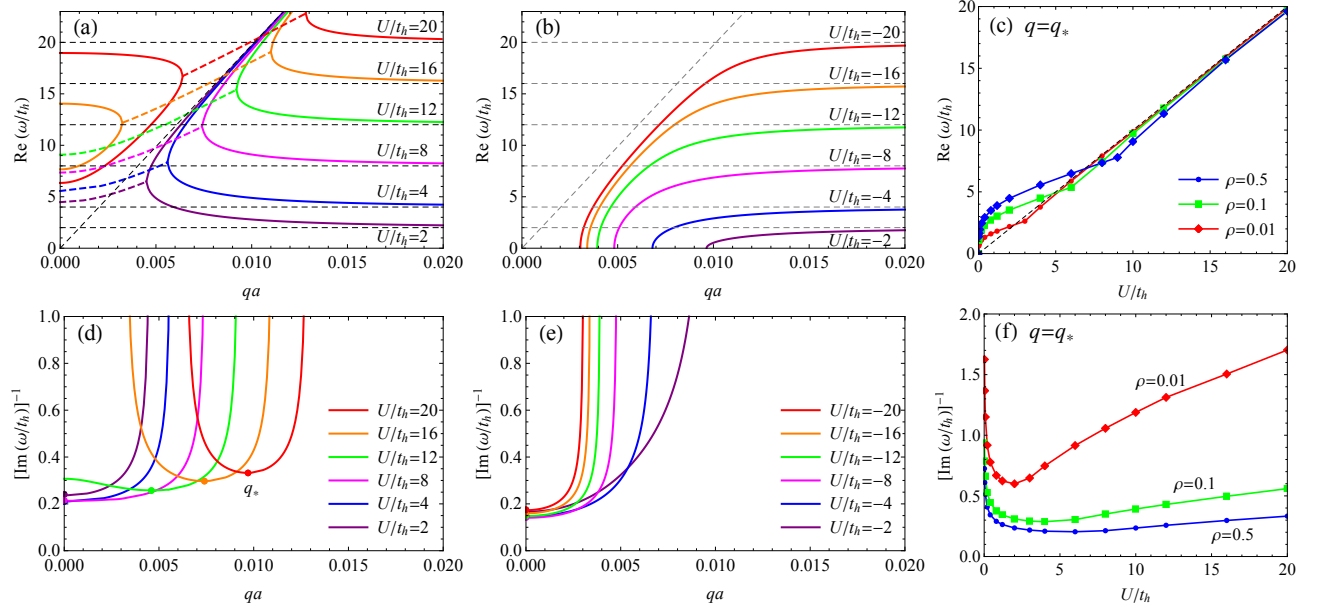


FIG. 2. (a), (b): Energy dispersion of the transverse electromagnetic field coupled to the η -pairing states in the Hubbard model. The solid curves show the real frequencies, while the dashed ones represent the real part of the complex frequencies. The sloped dashed line shows the dispersion relation in the vacuum ($\omega = cq$), and the horizontal dashed lines correspond to $\omega = |U|$. (c) Real part of ω at $q = q_*$, where the imaginary part takes the maximal value. The dashed line shows $\omega = U$. (d), (e): Inverse of the imaginary part of ω corresponding to the time scale of the growth of the dynamical instability. (f): Inverse of the imaginary part of ω at $q = q_*$. We set $\rho = 0.5$ in (a), (b), (d), (e) and $t_h = 1$ [eV] and $a = 1$ [Å] in (a)-(f).

($U < 0$), the solid curves show the real-frequency solutions, while the dashed curves represent the real part of the complex-frequency solutions. When U is positive and sufficiently large, there are two branches of the real solutions with the gaps near $q = 0$. As q increases, the two branches merge at some point, and turn into a conjugate pair of complex frequencies [46]. After going across the vacuum dispersion ($\omega = cq$), the solutions become real and split into two branches again. At high momentum, the two branches approach $\omega = cq$ and $\omega = U$. For $0 < U/t_h < 14.3$ ($\rho = 0.5$), the real branches near $q = 0$ vanish as discussed above, and only complex solutions exist at low momentum. For $U < 0$ [Fig. 2(b)], the dispersion shows a tachyonic spectrum. In general, we can prove that complex frequencies appear for all U and ρ [39], indicating that the electromagnetic field (and hence the η -pairing state) is always dynamically unstable.

In Figs. 2(d) and (e), we plot $[\text{Im}(\omega)]^{-1}$, i.e., the time scale of the growth of the instability. One can see that the shortest time scale among the \mathbf{q} modes (whose momentum is denoted by q_*) is of the order of \hbar/t_h , which is in the femtosecond regime. In the decaying process, the energy of the electromagnetic field is transferred from the binding energy of doublons for $U > 0$, and from the kinetic energy of doublons for $U < 0$. In the former, the doublons break up into two particles, while in the latter the doublons lose their momentum \mathbf{Q} . In both cases, the η -pairing states will eventually disappear.

For $U > 0$, the complex frequencies have nonzero real

parts [see Fig. 2(a)], so that the exponential growth of the electromagnetic field is accompanied by plasma oscillations. They induce intense light emission, where doublons' binding energies are released collectively. In Figs. 2(c) and (f), we plot $\text{Re} \omega$ and $[\text{Im} \omega]^{-1}$ at momentum q_* , corresponding to the characteristic frequency and the growing time scale of the dominant emitted light waves, respectively. The characteristic frequency is shifted from U . In particular, at $U \ll t_h$ it is proportional to $U^{1/4}$ with $q_* = 0$ [39]. As U increases, q_* starts to take a nonzero value around $U/t_h \approx 9$ [Fig. 2(d)], making a kink-like structure in Fig. 2(c). The time scale of the growth increases as the density decreases [Fig. 2(f)], but stays within the femtosecond regime even at $\rho = 0.01$. For $U < 0$, the decay of the η -pairing states is accompanied by unattenuated penetration of electromagnetic fields [39] in such a way that a tachyonic field grows exponentially as in order-parameter dynamics near critical points [47–49].

We emphasize that the mechanism of the plasma instability at $U > 0$ is different from that of spontaneous light emission, the latter of which is caused by a quantum-mechanical effect of electromagnetic fields and has the frequency $\omega = U$. The decay width of spontaneous emission is evaluated by $\Gamma = \frac{\omega}{3\pi\epsilon_0\hbar c^3} \sum_n |\langle \psi_N | J^\mu | \phi_n \rangle|^2$ [50], where ϵ_0 is the vacuum permittivity and the sum runs over all the eigenstates of the Hubbard model. For $\rho = 0.5$, $t_h = U = 1$ [eV], and $a = 1$ [Å], we have $\Gamma/M = 2.3 \times 10^7$ [s $^{-1}$] [39]. Thus, spontaneous emis-

sion takes place for each site in the time scale of 10^2 [ns], which is much slower than the plasma instability.

Summary and outlook.— We have shown that Yang’s η -pairing states have the intrinsic plasma instability for $U > 0$ and the tachyonic instability for $U < 0$ when the system is coupled to electromagnetic fields. The time scales of both of these instabilities are of the order of femtoseconds, which puts a strong constraint on the realization of the η -pairing states in real materials. The decay of the η -pairing states leads to enhanced light emission with characteristic frequencies shifted from the Hubbard interaction U for the repulsive case, and unattenuated penetration of electromagnetic fields for the attractive case. While we have focused on the simplest form of the η -pairing eigenstates (2), we expect that similar instabilities might exist for more general states having unpaired particles (at least if they are dilute enough). Stabilizing the η -pairing states coupled to electromagnetic fields is an interesting open problem, which merits further studies.

N.T. acknowledges support by KAKENHI Grant No. JP20K03811. M.N. acknowledges support by KAKENHI Grant No. JP20K14383. M.U. acknowledges support by KAKENHI Grant No. JP18H01145.

-
- [1] D. Fausti, R. I. Tobey, N. Dean, S. Kaiser, A. Dienst, M. C. Hoffmann, S. Pyon, T. Takayama, H. Takagi, and A. Cavalleri, *Science* **331**, 189 (2011).
 - [2] S. Kaiser, C. R. Hunt, D. Nicoletti, W. Hu, I. Gierz, H. Y. Liu, M. Le Tacon, T. Loew, D. Haug, B. Keimer, and A. Cavalleri, *Phys. Rev. B* **89**, 184516 (2014).
 - [3] W. Hu, S. Kaiser, D. Nicoletti, C. R. Hunt, I. Gierz, M. C. Hoffmann, M. Le Tacon, T. Loew, B. Keimer, and A. Cavalleri, *Nat. Mater.* **13**, 705 (2014).
 - [4] M. Mitrano, A. Cantaluppi, D. Nicoletti, S. Kaiser, A. Perucchi, S. Lupi, P. Di Pietro, D. Pontiroli, M. Riccò, S. R. Clark, D. Jaksch, and A. Cavalleri, *Nature* **530**, 461 (2016).
 - [5] A. Cantaluppi, M. Buzzi, G. Jotzu, D. Nicoletti, M. Mitrano, D. Pontiroli, M. Riccò, A. Perucchi, P. Di Pietro, and A. Cavalleri, *Nat. Phys.* **14**, 837 (2018).
 - [6] M. Buzzi, D. Nicoletti, M. Fechner, N. Tancogne-Dejean, M. A. Sentef, A. Georges, T. Biesner, E. Uykur, M. Dreschel, A. Henderson, T. Siegrist, J. A. Schlueter, K. Miyagawa, K. Kanoda, M.-S. Nam, A. Ardavan, J. Coulthard, J. Tindall, F. Schlawin, D. Jaksch, and A. Cavalleri, *Phys. Rev. X* **10**, 031028 (2020).
 - [7] M. Budden, T. Gebert, M. Buzzi, G. Jotzu, E. Wang, T. Matsuyama, G. Meier, Y. Laplace, D. Pontiroli, M. Riccò, F. Schlawin, D. Jaksch, A. Cavalleri, “Evidence for metastable photo-induced superconductivity in K_3C_{60} ”, arXiv:2002.12835.
 - [8] H. Oike, M. Kamitani, Y. Tokura, and F. Kagawa, *Sci. Adv.* **4**, eaau3489 (2018).
 - [9] H. Niwa, N. Yoshikawa, K. Tomari, R. Matsunaga, D. Song, H. Eisaki, and R. Shimano, *Phys. Rev. B* **100**, 104507 (2019).
 - [10] S. J. Zhang, Z. X. Wang, H. Xiang, X. Yao, Q. M. Liu, L. Y. Shi, T. Lin, T. Dong, D. Wu, and N. L. Wang, *Phys. Rev. X* **10**, 011056 (2020).
 - [11] M. Matsubara, Y. Okimoto, T. Ogasawara, Y. Tomioka, H. Okamoto, and Y. Tokura, *Phys. Rev. Lett.* **99**, 207401 (2007).
 - [12] A. S. McLeod, J. Zhang, M. Q. Gu, F. Jin, G. Zhang, K. W. Post, X. G. Zhao, A. J. Millis, W. B. Wu, J. M. Rondinelli, R. D. Averitt, and D. N. Basov, *Nat. Mater.* **19**, 397 (2020).
 - [13] L. Stojchevska, I. Vaskivskyi, T. Mertelj, P. Kusar, D. Svetin, S. Brazovskii, and D. Mihailovic, *Science* **344**, 177 (2014).
 - [14] I. Vaskivskyi, J. Gospodaric, S. Brazovskii, D. Svetin, P. Sutar, E. Goreshnik, I. A. Mihailovic, T. Mertelj, and D. Mihailovic, *Sci. Adv.* **1**, e1500168 (2015).
 - [15] K. Sun, S. Sun, C. Zhu, H. Tian, H. Yang, and J. Li, *Sci. Adv.* **4**, eaas9660 (2018).
 - [16] C. N. Yang, *Phys. Rev. Lett.* **63**, 2144 (1989).
 - [17] O. Vafeek, N. Regnault, and B. A. Bernevig, *SciPost Phys.* **3**, 043 (2017).
 - [18] D. K. Mark and O. I. Motrunich, *Phys. Rev. B* **102**, 075132 (2020).
 - [19] S. Moudgalya, N. Regnault, and B. A. Bernevig, *Phys. Rev. B* **102**, 085140 (2020).
 - [20] S. Kitamura and H. Aoki, *Phys. Rev. B* **94**, 174503 (2016).
 - [21] F. Peronaci, O. Parcollet, and M. Schiró, *Phys. Rev. B* **101**, 161101 (2020).
 - [22] M. W. Cook and S. R. Clark, *Phys. Rev. A* **101**, 033604 (2020).
 - [23] J. Tindall, F. Schlawin, M. A. Sentef, and D. Jaksch, *Phys. Rev. B* **103**, 035146 (2021).
 - [24] T. Kaneko, T. Shirakawa, S. Sorella, and S. Yunoki, *Phys. Rev. Lett.* **122**, 077002 (2019).
 - [25] T. Kaneko, S. Yunoki, and A. J. Millis, *Phys. Rev. Research* **2**, 032027 (2020).
 - [26] P. Werner, J. Li, D. Golež, and M. Eckstein, *Phys. Rev. B* **100**, 155130 (2019).
 - [27] J. Li, D. Golež, P. Werner, and M. Eckstein, *Phys. Rev. B* **102**, 165136 (2020).
 - [28] S. Diehl, A. Micheli, A. Kantian, B. Kraus, H. P. Büchler, and P. Zoller, *Nat. Phys.* **4**, 878 (2008).
 - [29] B. Kraus, H. P. Büchler, S. Diehl, A. Kantian, A. Micheli, and P. Zoller, *Phys. Rev. A* **78**, 042307 (2008).
 - [30] J.-S. Bernier, P. Barmettler, D. Poletti, and C. Kollath, *Phys. Rev. A* **87**, 063608 (2013).
 - [31] J. Tindall, B. Buča, J. R. Coulthard, and D. Jaksch, *Phys. Rev. Lett.* **123**, 030603 (2019).
 - [32] M. Nakagawa, N. Tsuji, N. Kawakami, and M. Ueda, to be published.
 - [33] G. Su, M.-L. Ge, and B.-H. Zhao, *Phys. Lett. A* **155**, 425 (1991).
 - [34] G. Su, M.-L. Ge, and B.-H. Zhao, *Phys. Stat. Sol. B* **173**, 709 (1992).
 - [35] C. N. Yang and S. C. Zhang, *Mod. Phys. Lett. B* **4**, 759 (1990).
 - [36] C. N. Yang, *Rev. Mod. Phys.* **34**, 694 (1962).
 - [37] J. R. Schrieffer, *Theory of Superconductivity* (Perseus, 1983).
 - [38] The diamagnetic component of the electromagnetic response function for the η -pairing states in the Hubbard model is given by

$$K_{\text{dia}}^{\mu\nu}(\mathbf{q}, \omega) \propto \delta_{\mu\nu} \sum_{\mathbf{k}\sigma} \frac{\partial^2 \varepsilon_{\mathbf{k}}}{\partial k_\mu^2} \langle \psi_N | c_{\mathbf{k}\sigma}^\dagger c_{\mathbf{k}\sigma} | \psi_N \rangle \propto \delta_{\mu\nu} \sum_{\mathbf{k}\sigma} \varepsilon_{\mathbf{k}} \langle \psi_N | c_{\mathbf{k}\sigma}^\dagger c_{\mathbf{k}\sigma} | \psi_N \rangle = 0, \text{ where } \varepsilon_{\mathbf{k}} = -2t_h \sum_{\mu=1}^3 \cos k_\mu \text{ is the single-particle band dispersion and } c_{\mathbf{k}\sigma} = \frac{1}{\sqrt{M}} \sum_j e^{-i\mathbf{k}\cdot\mathbf{R}_j} c_{j\sigma}.$$

- [39] See Supplementary Material for the details of the derivation of the electromagnetic response function for the η -pairing states and its properties including the symmetry constraint, the solution of the Maxwell equations, magnetic properties of tachyonic superconductors, and spontaneous light emission.
- [40] F. H. L. Essler, H. Frahm, F. Göhmann, A. Klümper, and V. E. Korepin, *The One-Dimensional Hubbard Model* (Cambridge University Press, 2005).
- [41] D. J. Scalapino, S. R. White, and S. Zhang, Phys. Rev. B **47**, 7995 (1993).
- [42] P. W. Anderson, Phys. Rev. **130**, 439 (1963).
- [43] R. Shimano and N. Tsuji, Annu. Rev. Condens. Matter Phys. **11**, 103 (2020).
- [44] Here, by “tachyonic”, we mean that the vacuum state is unstable since the system sits on a local maximum of a potential, and do not mean a hypothetical superluminal particle. When an ODLRO is present, a uniform magnetic field cannot exist [51, 52]. In other words, the energy dispersion of the electromagnetic field cannot cross the origin ($\omega = \mathbf{q} = 0$). To satisfy this condition, the system must be either a superconductor (with the dispersion of the electromagnetic field $\omega^2 \simeq c^2 q^2 + m^2 c^4$ with $m^2 > 0$) or a tachyonic superconductor ($\omega^2 \simeq c^2 q^2 + m^2 c^4$ with $m^2 < 0$).
- [45] The classification is rather formal here. To identify the nature of vortices in η pairing states, one has to go beyond the linear-response theory of the present analysis. The point at which λ exceeds ξ is, precisely speaking, not exactly at $|U| = 4t_h$ but very close to it [39].
- [46] This behavior is reminiscent of exceptional points in non-Hermitian systems [53].
- [47] T. W. B. Kibble, J. Phys. A: Math. Gen. **9**, 1387 (1976).
- [48] W. H. Zurek, Nature **317**, 505 (1985).
- [49] A. Polkovnikov, K. Sengupta, A. Silva, and M. Vengalattore, Rev. Mod. Phys. **83**, 863 (2011).
- [50] R. Loudon, *The Quantum Theory of Light*, 3rd ed. (Oxford University Press, New York, 2000).
- [51] G. L. Sewell, J. Stat. Phys. **61**, 415 (1990).
- [52] H. T. Nieh, G. Su, and B.-H. Zhao, Phys. Rev. B **51**, 3760 (1995).
- [53] Y. Ashida, Z. Gong, and M. Ueda, “Non-Hermitian Physics”, arXiv:2006.01837.
- [54] I. S. Gradshteyn and I. M. Ryzhik, *Table of Integrals, Series, and Products* (Academic Press, New York, 1995).

Supplemental Material for “Tachyonic and Plasma Instabilities of η -Pairing States Coupled to Electromagnetic Fields”

Naoto Tsuji^{1,2}, Masaya Nakagawa¹, and Masahito Ueda^{1,2,3}

¹*Department of Physics, University of Tokyo, Hongo, Tokyo 113-0033, Japan*

²*RIKEN Center for Emergent Matter Science (CEMS), Wako 351-0198, Japan*

³*Institute for Physics of Intelligence, University of Tokyo, Hongo, Tokyo 113-0033, Japan*

(Dated: February 1, 2022)

I. DERIVATION OF THE ELECTROMAGNETIC RESPONSE FUNCTION

In this section, we describe how to analytically evaluate the electromagnetic response function (Meissner kernel) [Eq. (3) in the main text],

$$K^{\mu\nu}(\mathbf{R}_j, t) = -i\theta(t)\langle\psi_N|[J^\mu(\mathbf{R}_j, t), J^\nu(0, 0)]|\psi_N\rangle, \quad (\text{S1})$$

at arbitrary lattice coordinate \mathbf{R}_j and time t for Yang's η -pairing state $|\psi_N\rangle$ [Eq. (4)] in the Hubbard model.

A. Reduction to the two-particle correlation function

The first step is to reduce the correlation function of N particles (S1) to that of two particles by shifting all the η operators in $|\psi_N\rangle$ to the left of the current operators using the commutation relation

$$[J^\mu(\mathbf{R}_j), \eta^+] = -2iet_h e^{i\mathbf{Q}\cdot\mathbf{R}_j} (c_{j+\mu\uparrow}^\dagger c_{j\downarrow}^\dagger + c_{j\uparrow}^\dagger c_{j+\mu\downarrow}^\dagger). \quad (\text{S2})$$

For convenience, we define the operator that appeared on the right-hand side of Eq. (S2) as

$$J_\eta^{\mu+}(\mathbf{R}_j) := -iet_h e^{i\mathbf{Q}\cdot\mathbf{R}_j} (c_{j+\mu\uparrow}^\dagger c_{j\downarrow}^\dagger + c_{j\uparrow}^\dagger c_{j+\mu\downarrow}^\dagger). \quad (\text{S3})$$

With this definition, we can write

$$[J^\mu(\mathbf{R}_j), \eta^+] = 2J_\eta^{\mu+}(\mathbf{R}_j). \quad (\text{S4})$$

Since $J_\eta^{\mu+}(\mathbf{R}_j)$ only involves creation operators, $J_\eta^{\mu+}(\mathbf{R}_j)$ commutes with η^+ . Therefore, we can repeatedly use the relation (S4) to obtain

$$[J^\mu(\mathbf{R}_j), (\eta^+)^n] = 2n(\eta^+)^{n-1} J_\eta^{\mu+}(\mathbf{R}_j) \quad (\text{S5})$$

for $n = 1, 2, \dots$. By using Eq. (S5), we can evaluate the current-current correlation function as

$$\begin{aligned} & \langle\psi_N|J^\mu(\mathbf{R}_j, t)J^\nu(0, 0)|\psi_N\rangle \\ &= \frac{1}{\sqrt{\mathcal{N}_N}} \langle\psi_N|J^\mu(\mathbf{R}_j, t)J^\nu(0, 0)(\eta^+)^{\frac{N}{2}}|0\rangle \\ &= \frac{1}{\sqrt{\mathcal{N}_N}} N \langle\psi_N|J^\mu(\mathbf{R}_j, t)(\eta^+)^{\frac{N}{2}-1}J_\eta^{\nu+}(0)|0\rangle \\ &= \frac{1}{\sqrt{\mathcal{N}_N}} N \langle\psi_N|(\eta^+)^{\frac{N}{2}-1}J^\mu(\mathbf{R}_j, t)J_\eta^{\nu+}(0)|0\rangle \\ &+ \frac{1}{\sqrt{\mathcal{N}_N}} N(N-2) \langle\psi_N|(\eta^+)^{\frac{N}{2}-2}J_\eta^{\mu+}(\mathbf{R}_j, t)J_\eta^{\nu+}(0)|0\rangle. \end{aligned} \quad (\text{S6})$$

Then, straightforward calculations show that

$$\langle\psi_N|(\eta^+)^{\frac{N}{2}-1} = \frac{1}{\sqrt{\mathcal{N}_N}} \frac{(\frac{N}{2})!(M-1)!}{(M-\frac{N}{2})!} \langle 0|\eta^-, \quad (\text{S7})$$

$$\langle\psi_N|(\eta^+)^{\frac{N}{2}-2} = \frac{1}{\sqrt{\mathcal{N}_N}} \frac{(\frac{N}{2})!(M-2)!}{2(M-\frac{N}{2})!} \langle 0|(\eta^-)^2, \quad (\text{S8})$$

which can be used to rewrite the correlation function (S6) as

$$\begin{aligned} & \langle\psi_N|J^\mu(\mathbf{R}_j, t)J^\nu(0, 0)|\psi_N\rangle \\ &= \frac{N}{\mathcal{N}_N} \frac{(\frac{N}{2})!(M-1)!}{(M-\frac{N}{2})!} \langle 0|\eta^- J^\mu(\mathbf{R}_j, t)J_\eta^{\nu+}(0)|0\rangle \\ &+ \frac{N(N-2)}{\mathcal{N}_N} \frac{(\frac{N}{2})!(M-2)!}{2(M-\frac{N}{2})!} \langle 0|(\eta^-)^2 J_\eta^{\mu+}(\mathbf{R}_j, t)J_\eta^{\nu+}(0)|0\rangle. \end{aligned} \quad (\text{S9})$$

To further simplify the expression, we use the commutation relations,

$$[\eta^-, J^\mu(\mathbf{R}_j)] = 2J_\eta^{\mu-}(\mathbf{R}_j), \quad (\text{S10})$$

$$[\eta^-, J_\eta^{\mu+}(\mathbf{R}_j)] = -J^\mu(\mathbf{R}_j), \quad (\text{S11})$$

where $J_\eta^{\mu-}(\mathbf{R}_j) := [J_\eta^{\mu+}(\mathbf{R}_j)]^\dagger$. Thus, the correlation function becomes

$$\begin{aligned} & \langle \psi_N | J^\mu(\mathbf{R}_j, t) J^\nu(0, 0) | \psi_N \rangle \\ &= \frac{2N}{\mathcal{N}_N} \frac{(\frac{N}{2})!(M-1)!}{(M-\frac{N}{2})!} \langle 0 | J_\eta^{\mu-}(\mathbf{R}_j, t) J_\eta^{\nu+}(0) | 0 \rangle \\ & \quad - \frac{N(N-2)}{\mathcal{N}_N} \frac{(\frac{N}{2})!(M-2)!}{2(M-\frac{N}{2})!} \langle 0 | \eta^- J^\mu(\mathbf{R}_j, t) J_\eta^{\nu+}(0) | 0 \rangle \\ &= \frac{2N(\frac{N}{2})!(M-2)!}{(M-\frac{N}{2}-1)!\mathcal{N}_N} \langle 0 | J_\eta^{\mu-}(\mathbf{R}_j, t) J_\eta^{\nu+}(0) | 0 \rangle. \end{aligned} \quad (\text{S12})$$

Here, let us recall that the normalization constant for the η -pairing state is explicitly given by

$$\mathcal{N}_N = \frac{(\frac{N}{2})!M!}{(M-\frac{N}{2})!}. \quad (\text{S13})$$

We use Eq. (S12) to reduce the current-current correlation function of N particles to that of two particles,

$$\begin{aligned} & \langle \psi_N | J^\mu(\mathbf{R}_j, t) J^\nu(0, 0) | \psi_N \rangle \\ &= 4C_{M,N} \langle 0 | J_\eta^{\mu-}(\mathbf{R}_j, t) J_\eta^{\nu+}(0) | 0 \rangle, \end{aligned} \quad (\text{S14})$$

where

$$C_{M,N} := \frac{\frac{N}{2}(M-\frac{N}{2})}{M(M-1)}. \quad (\text{S15})$$

Equation (S14) leads to Eq. (4) in the main text.

The technique used here (i.e., reduction of N -particle to few-particle correlation functions) can be applied not only to the electromagnetic response function (S1) but also to arbitrary correlation functions constructed from few-body operators.

B. Evaluation of the two-particle dynamics

In the previous subsection, we have shown that the N -particle correlation function (S1) can be reduced to the two-particle correlation function (S14). Since the two-particle problem in the Hubbard model is exactly solvable, we can evaluate the two-particle correlation function exactly. Here we describe the details of the evaluation.

First, we Fourier transform Eq. (S14) to obtain

$$\begin{aligned} & \sum_j e^{i\mathbf{q}\cdot\mathbf{R}_j} \langle \psi_N | J^\mu(\mathbf{R}_j, t) J^\nu(0, 0) | \psi_N \rangle \\ &= \frac{4}{M} C_{M,N} \langle 0 | J_\eta^{\mu-}(\mathbf{q}, t) J_\eta^{\nu+}(\mathbf{q}) | 0 \rangle, \end{aligned} \quad (\text{S16})$$

where

$$J_\eta^{\mu+}(\mathbf{q}) := \sum_j e^{-i\mathbf{q}\cdot\mathbf{R}_j} J_\eta^{\mu+}(\mathbf{R}_j), \quad (\text{S17})$$

$$J_\eta^{\mu-}(\mathbf{q}) := [J_\eta^{\mu+}(\mathbf{q})]^\dagger. \quad (\text{S18})$$

Acting $J_\eta^{\nu+}(\mathbf{q})$ on the vacuum state, we obtain

$$\begin{aligned} J_\eta^{\nu+}(\mathbf{q}) | 0 \rangle &= -iet_h \sum_j e^{i(\mathbf{Q}-\mathbf{q})\cdot\mathbf{R}_j} (c_{j+\nu\uparrow}^\dagger c_{j\downarrow}^\dagger + c_{j\uparrow}^\dagger c_{j+\nu\downarrow}^\dagger) | 0 \rangle \\ &= -iet_h \sum_j e^{i(\mathbf{Q}-\mathbf{q})\cdot\mathbf{R}_j} (|\mathbf{R}_j + \mathbf{e}_\nu, \mathbf{R}_j\rangle + |\mathbf{R}_j, \mathbf{R}_j + \mathbf{e}_\nu\rangle), \end{aligned} \quad (\text{S19})$$

where we have introduced the notation $|\mathbf{R}_j, \mathbf{R}_k\rangle := c_{j\uparrow}^\dagger c_{k\downarrow}^\dagger | 0 \rangle$ to represent a two-particle state with \uparrow spin at site j and \downarrow spin at site k , and \mathbf{e}_ν is the unit vector in the ν direction.

Since the system has the (discrete) translation symmetry, the center-of-mass (crystal) momentum of two particles under consideration is conserved. Let us define the translation operator T_μ that shifts two particles by one lattice site in the μ direction. We express the eigenstates of T_μ in terms of the center-of-mass momentum \mathbf{K} and the relative coordinate \mathbf{r} of the two particles as

$$|\mathbf{K}, \mathbf{r}\rangle = \frac{1}{\sqrt{M}} \sum_j e^{i\mathbf{K}\cdot\mathbf{R}_j} |\mathbf{R}_j + \mathbf{r}, \mathbf{R}_j\rangle, \quad (\text{S20})$$

which satisfies $T_\mu |\mathbf{K}, \mathbf{r}\rangle = e^{-i\mathbf{K}\cdot\mathbf{e}_\mu} |\mathbf{K}, \mathbf{r}\rangle$. Using the eigenstates (S20), $J_\eta^{\nu+}(\mathbf{q}) | 0 \rangle$ (S19) can be written as

$$\begin{aligned} J_\eta^{\nu+}(\mathbf{q}) | 0 \rangle &= -iet_h \sqrt{M} (|\mathbf{Q} - \mathbf{q}, +\mathbf{e}_\nu\rangle \\ & \quad + e^{-i(\mathbf{Q}-\mathbf{q})\cdot\mathbf{e}_\nu} |\mathbf{Q} - \mathbf{q}, -\mathbf{e}_\nu\rangle), \end{aligned} \quad (\text{S21})$$

which has the center-of-mass momentum $\mathbf{Q} - \mathbf{q}$. The action of the Hamiltonian in Eq. (1) in the main text on the state $|\mathbf{K}, \mathbf{r}\rangle$ (S20) is given by

$$\begin{aligned} H |\mathbf{K}, \mathbf{r}\rangle &= -t_h \sum_\mu [(1 + e^{i\mathbf{K}\cdot\mathbf{e}_\mu}) |\mathbf{K}, \mathbf{r} + \mathbf{e}_\mu\rangle \\ & \quad + (1 + e^{-i\mathbf{K}\cdot\mathbf{e}_\mu}) |\mathbf{K}, \mathbf{r} - \mathbf{e}_\mu\rangle] \\ & \quad + U(\delta_{\mathbf{r},0} - 1) |\mathbf{K}, \mathbf{r}\rangle. \end{aligned} \quad (\text{S22})$$

If we define operators Δ_μ^\pm that shift the relative coordinate of two particles by $\pm\mathbf{e}_\mu$, the Hamiltonian can be represented in the Hilbert subspace of two particles with the center-of-mass momentum \mathbf{K} as

$$\begin{aligned} H(\mathbf{K}) &= -t_h \sum_\mu [(1 + e^{i\mathbf{K}\cdot\mathbf{e}_\mu}) \Delta_\mu^+ + (1 + e^{-i\mathbf{K}\cdot\mathbf{e}_\mu}) \Delta_\mu^-] \\ & \quad + U(\delta_{\mathbf{r},0} - 1). \end{aligned} \quad (\text{S23})$$

Using the representation (S23), the correlation function (S16) can be written as

$$\begin{aligned} & \sum_j e^{i\mathbf{q}\cdot\mathbf{R}_j} \langle \psi_N | J^\mu(\mathbf{R}_j, t) J^\nu(0, 0) | \psi_N \rangle \\ &= \frac{4}{M} C_{M,N} \langle 0 | J_\eta^{\mu-}(\mathbf{q}) e^{-iH(\mathbf{Q}-\mathbf{q})t} J_\eta^{\nu+}(\mathbf{q}) | 0 \rangle. \end{aligned} \quad (\text{S24})$$

Without loss of generality, we assume that \mathbf{q} is parallel to the z direction [$\mathbf{q} = (0, 0, q)$]. Then,

$$H(\mathbf{Q} - \mathbf{q}) = -t_h[(1 - e^{-iq})\Delta_z^+ + (1 - e^{iq})\Delta_z^-] + U(\delta_{\mathbf{r},0} - 1). \quad (\text{S25})$$

Hence, the two-particle dynamics that we have to consider is essentially a one-dimensional problem, in which the relative coordinates r_x and r_y are conserved. Below, we decompose the electromagnetic response function into the transverse component $K^\perp(\mathbf{q}, \omega) := K^{\mu\mu}(\mathbf{q}, \omega)$ ($\mu = x, y$) and the longitudinal one $K^\parallel(\mathbf{q}, \omega) := K^{zz}(\mathbf{q}, \omega)$. The off-diagonal components are absent, i.e., $K^{\mu\nu}(\mathbf{q}, \omega) = 0$ for $\mu \neq \nu$, since the state $e^{-iH(\mathbf{Q}-\mathbf{q})t}J_{\eta}^{\nu+}(\mathbf{q})|0\rangle$ never has an overlap with the state $J_{\eta}^{\mu+}|0\rangle$ for $\mu \neq \nu$.

C. Transverse component

For the transverse component, the two-particle state $J_{\eta}^{\nu+}(\mathbf{q})|0\rangle$ (S21) has the relative coordinates, $(r_x, r_y) \neq (0, 0)$. Since r_x and r_y are conserved during the time evolution, the two particles do not sit on the same site. Therefore, they do not interact with each other, and the dynamics becomes effectively noninteracting. The correlation function (S16) now reads

$$\begin{aligned} & \sum_j e^{i\mathbf{q} \cdot \mathbf{R}_j} \langle \psi_N | J^\mu(\mathbf{R}_j, t) J^\mu(0, 0) | \psi_N \rangle \quad (\mu = x, y) \\ &= 4e^2 t_h^2 C_{M,N} \sum_{s=\pm} \langle \mathbf{Q} - \mathbf{q}, s\mathbf{e}_\mu | e^{-iH(\mathbf{Q}-\mathbf{q})t} | \mathbf{Q} - \mathbf{q}, s\mathbf{e}_\mu \rangle, \end{aligned} \quad (\text{S26})$$

where

$$H(\mathbf{Q} - \mathbf{q}) = -t_h[(1 - e^{-iq})\Delta_z^+ + (1 - e^{iq})\Delta_z^-] - U \quad (\text{S27})$$

is the noninteracting Hamiltonian which can be diagonalized by Fourier transformation with respect to the relative coordinate r_z . The result is

$$\begin{aligned} & \sum_j e^{i\mathbf{q} \cdot \mathbf{R}_j} \langle \psi_N | J^\mu(\mathbf{R}_j, t) J^\mu(0, 0) | \psi_N \rangle \quad (\mu = x, y) \\ &= 8e^2 t_h^2 C_{M,N} \frac{e^{iUt}}{M} \sum_{\mathbf{k}} e^{2it_h(\cos k_z - \cos(k_z + q))t} \\ &= 8e^2 t_h^2 C_{M,N} e^{iUt} \int_{-\pi}^{\pi} \frac{dk_z}{2\pi} e^{2it_h(\cos k_z - \cos(k_z + q))t} \\ &= 8e^2 t_h^2 C_{M,N} e^{iUt} J_0\left(4t_h \sin \frac{q}{2} t\right), \end{aligned} \quad (\text{S28})$$

where $J_0(x)$ is the zeroth-order Bessel function of the first kind. We thus obtain the transverse component of the electromagnetic response function as

$$K^\perp(\mathbf{q}, t) = -8i\theta(t)e^2 t_h^2 C_{M,N} (e^{iUt} - e^{-iUt}) \times J_0\left(4t_h \sin \frac{q}{2} t\right). \quad (\text{S29})$$

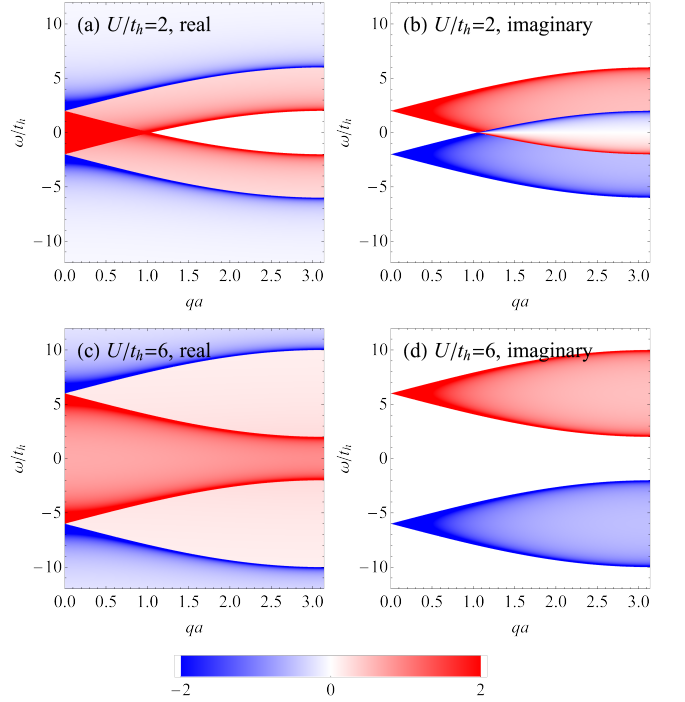


FIG. S1. Transverse component $K^\perp(\mathbf{q}, \omega)$ of the electromagnetic response function for the η -pairing states in the Hubbard model in units of $4e^2 t_h C_{M,N}$. (a), (b): Real (a) and imaginary (b) parts of $K^\perp(\mathbf{q}, \omega)$ for $U/t_h = 2$. (c), (d): Real (c) and imaginary (d) parts of $K^\perp(\mathbf{q}, \omega)$ for $U/t_h = 6$.

Using the integral formula for the Bessel function ($a > 0$),

$$\int_0^\infty dt e^{i\omega t} J_0(at) = \begin{cases} \frac{i \text{sgn}(\omega)}{\sqrt{\omega^2 - a^2}} & \text{for } |\omega| > a; \\ \frac{1}{\sqrt{a^2 - \omega^2}} & \text{for } |\omega| < a, \end{cases} \quad (\text{S30})$$

we obtain

$$K^\perp(\mathbf{q}, \omega) = -8ie^2 t_h C_{M,N} \left[f_q\left(\frac{\omega + U}{t_h}\right) - f_q\left(\frac{\omega - U}{t_h}\right) \right], \quad (\text{S31})$$

where

$$f_q(x) := \begin{cases} \frac{i \text{sgn}(x)}{\sqrt{x^2 - 16 \sin^2 \frac{q}{2}}} & \text{for } |x| > 4 \sin \frac{q}{2}; \\ \frac{1}{\sqrt{16 \sin^2 \frac{q}{2} - x^2}} & \text{for } |x| < 4 \sin \frac{q}{2}. \end{cases} \quad (\text{S32})$$

This is the final result for the transverse component in Eq. (5) in the main text.

In Fig. S1, we plot $K^\perp(\mathbf{q}, \omega)$ for $U/t_h = 2$ and 6. The imaginary part of $K^\perp(\mathbf{q}, \omega)$ represents the absorption (emission) of light for the η -pairing states. When a doublon decays by emitting light with momentum \mathbf{q} , quasiparticles with momentum \mathbf{k} and $-\mathbf{k} + \mathbf{Q} - \mathbf{q}$ are created. As discussed above, these particles never interact with each other, so that the total energy of the two particles is given by $-2t_h \sum_{\mu} [(\cos k_{\mu}) + \cos(-k_{\mu} + Q_{\mu} - q_{\mu})] = -4t_h \sin \frac{q}{2} \sin(k_z + \frac{q}{2})$. The energy of quasiparticles ranges from $-4t_h \sin \frac{q}{2}$ to $4t_h \sin \frac{q}{2}$. Since the energy

of a single doublon is U , the condition for light emission to take place is $|\omega - U| < 4t_h \sin \frac{q}{2}$. This is exactly the condition of $\text{Im} K^\perp(\mathbf{q}, \omega) > 0$ (for $U/t_h > 4$). The gap for the electromagnetic response function closes at $q = \pi$ when $U/t_h = 4$.

D. Asymptotic behavior at long distance

Here we derive the asymptotic behavior of the transverse electromagnetic response function (S31) at long distance and low frequency, which is related to Pippard's coherence length. In the low-frequency limit, the kernel is given by

$$K^\perp(\mathbf{q}, \omega = 0) = 16e^2 t_h^2 C_{M,N} \begin{cases} \frac{\text{sgn}(U)}{\sqrt{U^2 - 16t_h^2 \sin^2 \frac{q}{2}}} & \text{for } |U| > 4t_h \sin \frac{q}{2}; \\ 0 & \text{for } |U| < 4t_h \sin \frac{q}{2}. \end{cases} \quad (\text{S33})$$

We consider the problem in two distinct regimes: $|U| > 4t_h$ and $|U| < 4t_h$.

In the first case ($|U| > 4t_h$), the Fourier transform of $K^\perp(\mathbf{q}, \omega = 0)$ (S33) to real space in the z direction reads

$$K^\perp(j, \omega = 0) = 16e^2 t_h^2 C_{M,N} \int_{-\pi}^{\pi} \frac{dq}{2\pi} e^{iqj} \frac{\text{sgn}(U)}{\sqrt{U^2 - 16t_h^2 \sin^2 \frac{q}{2}}}. \quad (\text{S34})$$

Precisely speaking, Eq. (S34) shows the electromagnetic response function for $q_x = q_y = 0$, $R_z = j$, and $\omega = 0$. The asymptotic behavior of $K^\perp(j, \omega = 0)$ for $j \gg 1$ is qualitatively similar to that of $K^\perp(\mathbf{R}_j, \omega = 0)$ (i.e., the full Fourier transform of $K^\perp(\mathbf{q}, \omega = 0)$ in all directions) for $|\mathbf{R}_j| \gg 1$, since the dominant contribution in $K^\perp(j, \omega = 0) = \sum_{R_x, R_y} K^\perp(R_x, R_y, R_z = j, \omega = 0)$ for $j \gg 1$ arises near $R_x \sim R_y \sim 0$. In particular, if $K^\perp(\mathbf{R}_j, \omega = 0)$ decays exponentially for $|\mathbf{R}_j| \gg 1$, then $K^\perp(j, \omega = 0)$ (S34) also decays exponentially for $j \gg 1$ with the same correlation length.

The integral in Eq. (S34) can be evaluated analytically as

$$K^\perp(j, \omega = 0) = 16e^2 t_h^2 C_{M,N} \frac{\text{sgn}(U)}{\sqrt{U^2 - 16t_h^2}} \times \frac{{}_3F_2(\frac{1}{2}, \frac{1}{2}, 1; 1-j, 1+j; \frac{1}{1-U^2/16t_h^2})}{\Gamma(1-j)\Gamma(1+j)}, \quad (\text{S35})$$

where ${}_3F_2(a_1, a_2, a_3; b_1, b_2; z)$ is the generalized hypergeometric function [54], and $\Gamma(z)$ is the gamma function. The explicit expression (S35), however, does not directly tell us about the long-distance behavior. Hence we take a different approach.

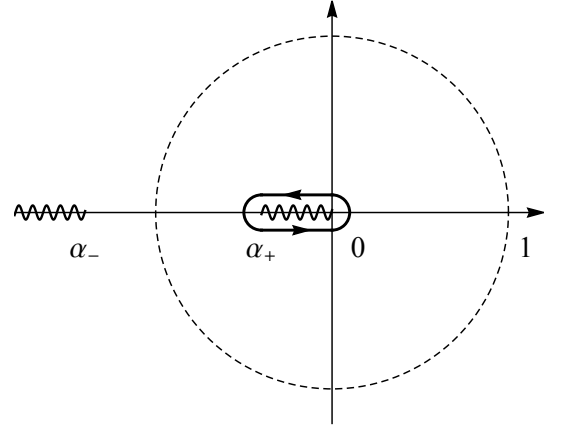


FIG. S2. Contour for the integral (S39) in the complex plane depicted by the dashed circle, which can continuously be deformed to the solid curve without crossing the branch cuts shown by the wavy lines.

The kernel (S34) can be written as

$$K^\perp(j, \omega = 0) = 4e^2 t_h C_{M,N} \text{sgn}(U) I_j(u), \quad (\text{S36})$$

where

$$u = \frac{|U|}{4t_h} \quad (\text{S37})$$

is the normalized interaction strength, and

$$I_j(u) := \int_{-\pi}^{\pi} \frac{dq}{2\pi} e^{-iqj} \frac{1}{\sqrt{u^2 - \sin^2 \frac{q}{2}}} \quad (\text{S38})$$

for $u > 1$. By putting $z = e^{-iq}$, we transform the integral (S38) to a complex contour integral,

$$I_j(u) = \oint \frac{dz}{2\pi i} z^{j-1} \frac{1}{\sqrt{u^2 - \frac{1}{2}(1 - \frac{1}{2}(z + z^{-1}))}} = 2 \oint \frac{dz}{2\pi i} \frac{z^{j-\frac{1}{2}}}{\sqrt{z^2 + 2(2u^2 - 1)z + 1}}, \quad (\text{S39})$$

where the contour is taken to be the circle around the origin with unit radius $|z| = 1$ (dashed curve in Fig. S2). In the case of $|U| > 4t_h$, we have $u > 1$. The roots of the quadratic polynomial in the denominator of (S39) are given by

$$\alpha_{\pm} = 1 - 2u^2 \pm \sqrt{(2u^2 - 1)^2 - 1}, \quad (\text{S40})$$

which are real numbers. These roots satisfy $\alpha_- < -1 < \alpha_+ < 0$ and $\alpha_+ \alpha_- = 1$. Using α_{\pm} , we can write the contour integral (S39) as

$$I_j(u) = 2 \oint \frac{dz}{2\pi i} \frac{z^{j-\frac{1}{2}}}{\sqrt{(z - \alpha_+)(z - \alpha_-)}}. \quad (\text{S41})$$

In Fig. S2, we show the branch cuts that we adopt in evaluating Eq. (S41) by wavy lines. With this configuration, the contour can be smoothly deformed to the solid curve in Fig. S2 without crossing the branch cuts, where the integral is evaluated as

$$\begin{aligned} I_j(u) &= 2(e^{i(j-\frac{1}{2})\pi+i\pi} - e^{i(j-\frac{1}{2})\pi}) \\ &\times \int_{\alpha_+}^0 \frac{dx}{2\pi i} \frac{(-x)^{j-\frac{1}{2}}}{\sqrt{(x-\alpha_+)(x-\alpha_-)}} \\ &= -4e^{i(j-\frac{1}{2})\pi} \int_{\alpha_+}^0 \frac{dx}{2\pi i} \frac{(-x)^{j-\frac{1}{2}}}{\sqrt{(x-\alpha_+)(x-\alpha_-)}}. \end{aligned} \quad (\text{S42})$$

The asymptotic behavior of $I_j(u)$ can be read off as follows: for $j \gg 1$, the function $\frac{(-x)^{j-\frac{1}{2}}}{\sqrt{x-\alpha_+}}$ in the integrand has a concentrated contribution near $x = \alpha_+$, while $\frac{1}{\sqrt{x-\alpha_-}}$ is a smooth function in $(\alpha_+, 0]$. Therefore, one can replace $\frac{1}{\sqrt{x-\alpha_-}}$ by $\frac{1}{\sqrt{\alpha_+-\alpha_-}}$ in the integrand of Eq. (S42), obtaining

$$I_j(u) \approx -4e^{i(j-\frac{1}{2})\pi} \frac{1}{\sqrt{\alpha_+-\alpha_-}} \int_{\alpha_+}^0 \frac{dx}{2\pi i} \frac{(-x)^{j-\frac{1}{2}}}{\sqrt{x-\alpha_+}} \quad (\text{S43})$$

for $j \gg 1$. The rest of the integral can be evaluated as

$$\begin{aligned} I_j(u) &\approx -4e^{i(j-\frac{1}{2})\pi} \frac{1}{\sqrt{\alpha_+-\alpha_-}} \frac{1}{2\pi i} \frac{\sqrt{\pi}\Gamma(j+\frac{1}{2})}{\Gamma(j+1)} (-\alpha_+)^j \\ &= \frac{2}{\sqrt{\pi}} \frac{1}{\sqrt{\alpha_+-\alpha_-}} \frac{\Gamma(j+\frac{1}{2})}{\Gamma(j+1)} \alpha_+^j. \end{aligned} \quad (\text{S44})$$

Using Stirling's formula, we obtain the asymptotic form of $I_j(u)$ as

$$I_j(u) \approx \frac{2}{\sqrt{\pi}} \frac{1}{\sqrt{\alpha_+-\alpha_-}} \frac{1}{\sqrt{j}} \alpha_+^j. \quad (\text{S45})$$

Thus, the transverse electromagnetic response function behaves in the long distance ($j \rightarrow \infty$) as

$$K^\perp(j, \omega = 0) \approx \cos nt. \times \frac{\alpha_+^j}{\sqrt{j}}. \quad (\text{S46})$$

Since $|\alpha_+| < 1$, $K^\perp(j, \omega = 0)$ decays exponentially in space with Pippard's coherence length ξ defined by

$$K^\perp(j, \omega = 0) \approx \text{const.} \times \exp\left(-\frac{j}{\xi}\right). \quad (\text{S47})$$

Physically, ξ represents the length scale over which a response against a local perturbation of electromagnetic fields propagates in space (Pippard's nonlocal electrodynamics [37]).

From the result (S46), ξ is identified as

$$\xi = -\frac{a}{\ln|\alpha_+|} = \frac{a}{\cosh^{-1}(2u^2-1)}, \quad (\text{S48})$$

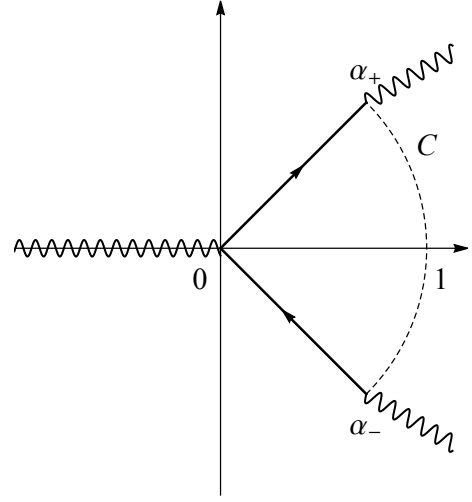


FIG. S3. Contour C for the integral (S52) in the complex plane depicted by the dashed arc, which can continuously be deformed to the solid lines without crossing the branch cuts as shown by the wavy lines.

which does not depend on the doublon density ρ . At $|U| = 4t_h =: U_c$, the coherence length diverges as

$$\xi \propto \frac{1}{|U - U_c|^{\frac{1}{2}}}. \quad (\text{S49})$$

This is exactly the point where the electromagnetic gap closes at $q = \pi$.

In the second case ($|U| < 4t_h$), the Meissner kernel in the low-frequency limit is expressed as

$$K^\perp(j, \omega = 0) = 4e^2 t_h C_{M,N} \text{sgn}(U) I_j(u) \quad (\text{S50})$$

with

$$I_j(u) = \int_{u \geq |\sin \frac{q}{2}|} \frac{dq}{2\pi} e^{-iqj} \frac{1}{\sqrt{u^2 - \sin^2 \frac{q}{2}}} \quad (\text{S51})$$

for $u < 1$. Similarly to the first case, we put $z = e^{-iq}$ to rewrite the integral (S51) as

$$I_j(u) = 2 \int_C \frac{dz}{2\pi i} \frac{z^{j-\frac{1}{2}}}{\sqrt{(z-\alpha_+)(z-\alpha_-)}}, \quad (\text{S52})$$

where the roots in the denominator are given by

$$\alpha_{\pm} = 1 - 2u^2 \pm i\sqrt{1 - (2u^2 - 1)^2}, \quad (\text{S53})$$

and the contour C is taken to be the arc of the circle with the unit radius connecting α_- and α_+ (dashed curve in Fig. S3). We choose the branch cuts in the integrand of Eq. (S52) as shown by wavy lines in Fig. S3.

Following the steepest descent method, we deform the contour from C to the solid lines in Fig. S3 without crossing the branch cuts, where we put $z = r\alpha_{\pm}$. Now the

integral (S52) can be evaluated as

$$I_j(u) = 2 \int_0^1 \frac{dr}{2\pi i} \alpha_+ \frac{(r\alpha_+)^{j-\frac{1}{2}}}{\sqrt{(r\alpha_+ - \alpha_+)(r\alpha_+ - \alpha_-)}} - 2 \int_0^1 \frac{dr}{2\pi i} \alpha_- \frac{(r\alpha_-)^{j-\frac{1}{2}}}{\sqrt{(r\alpha_- - \alpha_+)(r\alpha_- - \alpha_-)}}. \quad (\text{S54})$$

For $j \gg 1$, the function $\frac{r^{j-\frac{1}{2}}}{\sqrt{r\alpha_+ - \alpha_+}}$ in the first integral is dominantly contributed from a region near $r = 1$, which allows us to replace $\frac{1}{\sqrt{r\alpha_+ - \alpha_-}}$ by $\frac{1}{\sqrt{\alpha_+ - \alpha_-}}$ in the integrand. A similar approximation can be applied to the second term. Taking care of the branch cuts, we obtain

$$I_j(u) \approx \frac{2(\alpha_+^j e^{\frac{i\pi}{4}} - \alpha_-^j e^{-\frac{i\pi}{4}})}{\sqrt{|\alpha_+ - \alpha_-|}} \int_0^1 \frac{dr}{2\pi i} \frac{r^{j-\frac{1}{2}}}{\sqrt{1-r}}. \quad (\text{S55})$$

If we define $\alpha_{\pm} =: e^{\pm i\varphi}$, the integral (S51) can be approximated as

$$I_j(u) \approx \frac{2 \sin(j\varphi + \frac{\pi}{4})}{\sqrt{\pi} \sqrt{|\alpha_+ - \alpha_-|}} \frac{\Gamma(j + \frac{1}{2})}{\Gamma(j + 1)}. \quad (\text{S56})$$

Using Stirling's formula, the asymptotic form of $I_j(u)$ for $j \gg 1$ is given by

$$I_j(u) \approx \frac{2 \sin(j\varphi + \frac{\pi}{4})}{\sqrt{\pi} \sqrt{|\alpha_+ - \alpha_-|}} \frac{1}{\sqrt{j}}. \quad (\text{S57})$$

Therefore, the kernel decays in a long distance according to a power law as

$$K^{\perp}(j, \omega = 0) \approx \text{const.} \times \frac{1}{\sqrt{j}}. \quad (\text{S58})$$

This means that the coherence length diverges ($\xi = \infty$) for $|U| < 4t_h$.

In Fig. S4, we plot the coherence length ξ for the η -pairing states with $t_h = 1$ [eV], $a = 1$ [Å], and $\rho = 0.5$ in comparison with London's penetration depth defined by $\lambda = \sqrt{\frac{\hbar^2 a U}{16\mu_0 e^2 t_h^2 C_{M,N}}}$. At $0 \leq U < 4t_h$, λ grows smoothly as a function of U , and satisfies $\lambda < \xi = \infty$. When U exceeds $4t_h$, ξ immediately decays to the order of 1 [Å], whereas λ stays on the order of 10 [nm]. The point at which λ becomes equal to ξ is very close to $U = 4t_h$, beyond which λ becomes larger than ξ . Thus, for $0 \leq U < 4t_h$ the η -pairing state is a type-I superconductor, whereas for $U > 4t_h$ the η -pairing state is classified to a type-II superconductor.

For $U < 0$, we analytically continue λ to complex values, which has a physical meaning as discussed in Sec. . We will see that the η -pairing state has different magnetic properties depending on whether $|\lambda|$ is larger than ξ or not. For $-4t_h < U < 0$, we have the relation $|\lambda| < \xi$, where the η -pairing state is called a type-I tachyonic superconductor (see the main text). For $U < -4t_h$, we have $|\lambda| > \xi$, where the η -pairing state is called a type-II tachyonic superconductor (see the phase diagram in Fig. 1(b) in the main text).

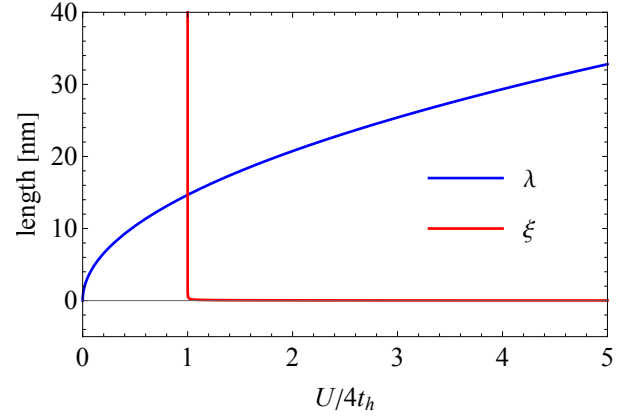


FIG. S4. Comparison between London's penetration depth λ and Pippard's coherence length ξ for the η -pairing states in the Hubbard model with $t_h = 1$ [eV], $a = 1$ [Å], and $\rho = 0.5$.

E. Longitudinal component

The longitudinal component of the electromagnetic response function is defined by $K^{\parallel}(\mathbf{q}, \omega) := K^{zz}(\mathbf{q}, \omega)$, where we take $\mathbf{q} \parallel \mathbf{e}_z$. The zz component of the current-current correlation function (S14) reads

$$\begin{aligned} & \sum_j e^{i\mathbf{q} \cdot \mathbf{R}_j} \langle \psi_N | J^z(\mathbf{R}_j, t) J^z(0, 0) | \psi_N \rangle \\ &= 4e^2 t_h^2 C_{M,N} (\langle \mathbf{Q} - \mathbf{q}, +\mathbf{e}_z | - e^{-iq} \langle \mathbf{Q} - \mathbf{q}, -\mathbf{e}_z |) \\ & \quad \times e^{-iH(\mathbf{Q}-\mathbf{q})t} (| \mathbf{Q} - \mathbf{q}, +\mathbf{e}_z \rangle - e^{iq} | \mathbf{Q} - \mathbf{q}, -\mathbf{e}_z \rangle), \end{aligned} \quad (\text{S59})$$

where $H(\mathbf{Q} - \mathbf{q})$ is given in Eq. (S25). During the time evolution, the relative coordinate of two particles changes only in the z direction. Therefore, what we need to solve is essentially a one-dimensional two-particle problem, which can be solved exactly in the spirit of the Bethe ansatz [40]. Here we do not go into details of analytical solutions, since we can easily diagonalize the Hamiltonian (S25) numerically for a large system size.

In Fig. S5, we plot $K^{\parallel}(\mathbf{q}, \omega)$ for $U/t_h = 2$ and 6. Compared with the transverse component (Fig. S1), there appear sideband structures which are shifted by U from the original bands in the longitudinal component due to the effect of the interaction. Otherwise, both of them have similar spectral features. In the low-frequency limit, the longitudinal component vanishes,

$$\lim_{\omega \rightarrow 0} K^{\parallel}(\mathbf{q}, \omega) = 0, \quad (\text{S60})$$

as required by charge conservation (see Sec.). In the low-momentum limit, the longitudinal component agrees with the transverse one,

$$\begin{aligned} \lim_{\mathbf{q} \rightarrow 0} K^{\parallel}(\mathbf{q}, \omega) &= \lim_{\mathbf{q} \rightarrow 0} K^{\perp}(\mathbf{q}, \omega) \\ &= 8e^2 t_h^2 C_{M,N} \left(\frac{1}{\omega + U} - \frac{1}{\omega - U} \right), \end{aligned} \quad (\text{S61})$$

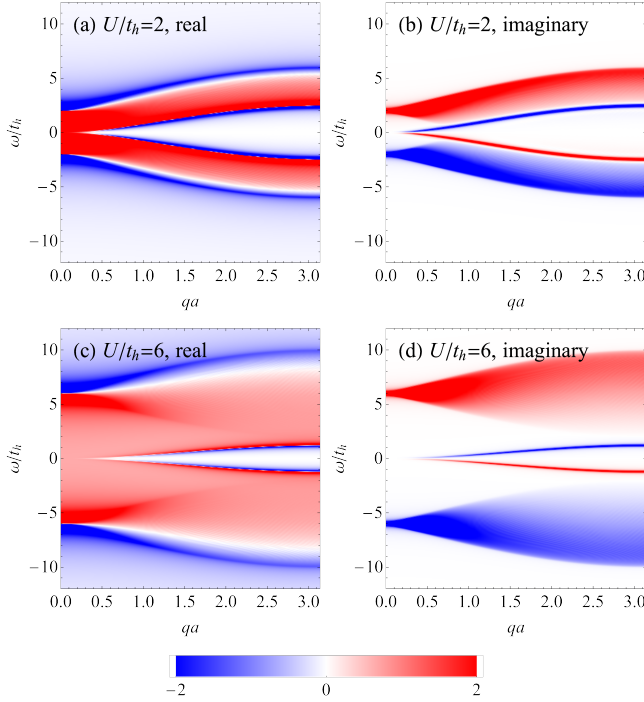


FIG. S5. Longitudinal component $K^{\parallel}(\mathbf{q}, \omega)$ of the electromagnetic response function for the η -pairing states in the Hubbard model in units of $4e^2 t_h C_{M,N}$. (a), (b): Real (a) and imaginary (b) parts of $K^{\parallel}(\mathbf{q}, \omega)$ for $U/t_h = 2$. (c), (d): Real (c) and imaginary (d) parts of $K^{\parallel}(\mathbf{q}, \omega)$ for $U/t_h = 6$.

since the hopping in the z direction is suppressed in the limit of $\mathbf{q} \rightarrow 0$ as can be seen from Eq. (S25).

II. CHARGE CONSERVATION

In the Hubbard model [Eq. (1) in the main text], electric charge is conserved due to the charge $U(1)$ symmetry. This imposes a nontrivial constraint on the electromagnetic response function [37]. To see this, we introduce the four-vector form of the electromagnetic response function defined by

$$K^{\mu\nu}(\mathbf{q}, \omega) = -i\theta(t) \langle \psi_N | [J^\mu(\mathbf{R}_j, t), J^\nu(0, 0)] | \psi_N \rangle \quad (\text{S62})$$

($\mu, \nu = 0, x, y, z$), where $J^\mu(\mathbf{R}_j) = (c\rho(\mathbf{R}_j), \mathbf{J}(\mathbf{R}_j))$ is the four-vector current, and

$$\rho(\mathbf{R}_j) = e \sum_{\sigma} c_{j\sigma}^\dagger c_{j\sigma} \quad (\text{S63})$$

is the local density operator. In the following, we use the metric convention $\eta^{\mu\nu} = \text{diag}(-, +, +, +)$. The linear response in the four-vector form reads $J^\mu(\mathbf{q}, \omega) = -K^{\mu\nu}(\mathbf{q}, \omega) A_\nu(\mathbf{q}, \omega)$, where $A_\nu = \eta_{\nu\lambda} A^\lambda = (-\frac{\phi}{e}, \mathbf{A})$ and ϕ is the scalar potential.

A. Charge response function

The charge response function for the η -pairing state is given by

$$K^{00}(\mathbf{R}_j, t) = -ic^2\theta(t) \langle \psi_N | [\rho(\mathbf{R}_j, t), \rho(0, 0)] | \psi_N \rangle. \quad (\text{S64})$$

As before, the density-density correlation function for N particles can be reduced to the two-particle correlation function. To see this, we define local η operators,

$$\eta^+(\mathbf{R}_j) := e^{i\mathbf{Q} \cdot \mathbf{R}_j} c_{j\uparrow}^\dagger c_{j\downarrow}^\dagger, \quad (\text{S65})$$

$$\eta^-(\mathbf{R}_j) := e^{-i\mathbf{Q} \cdot \mathbf{R}_j} c_{j\downarrow} c_{j\uparrow}. \quad (\text{S66})$$

They satisfy the following commutation relations:

$$[\rho(\mathbf{R}_j), \eta^\pm] = \pm 2\eta^\pm(\mathbf{R}_j), \quad (\text{S67})$$

$$[\eta^\pm(\mathbf{R}_j), \eta^\pm] = 0, \quad (\text{S68})$$

$$[\eta^\pm(\mathbf{R}_j), \eta^\mp] = \pm(\rho(\mathbf{R}_j) - 1). \quad (\text{S69})$$

Applying the above relations iteratively, we can reduce the N -particle density-density correlation function to

$$\begin{aligned} & \langle \psi_N | \rho(\mathbf{R}_j, t) \rho(0, 0) | \psi_N \rangle \\ &= 4e^2 C_{M,N} \langle 0 | \eta^-(\mathbf{R}_j, t) \eta^+(0, 0) | 0 \rangle + 4e^2 \frac{\frac{N}{2}(\frac{N}{2} - 1)}{M(M - 1)}. \end{aligned} \quad (\text{S70})$$

From this result, we can evaluate the charge response function as

$$\begin{aligned} K^{00}(\mathbf{q}, t) &= -4i\theta(t) c^2 e^2 t_h^2 C_{M,N} \\ &\times [\langle \mathbf{Q} - \mathbf{q}, \mathbf{r} = 0 | e^{-iH(\mathbf{Q}-\mathbf{q})t} | \mathbf{Q} - \mathbf{q}, \mathbf{r} = 0 \rangle \\ &- \langle \mathbf{Q} + \mathbf{q}, \mathbf{r} = 0 | e^{iH(\mathbf{Q}+\mathbf{q})t} | \mathbf{Q} + \mathbf{q}, \mathbf{r} = 0 \rangle], \end{aligned} \quad (\text{S71})$$

where

$$\begin{aligned} H(\mathbf{Q} \pm \mathbf{q}) &= -t_h((1 - e^{\pm iq})\Delta_z^+ + (1 - e^{\mp iq})\Delta_z^-) \\ &+ U(\delta_{\mathbf{r},0} - 1). \end{aligned} \quad (\text{S72})$$

Thus, the problem reduces to solving the two-particle dynamics in the one-dimensional Hubbard model, which can be diagonalized numerically or analytically with the Bethe ansatz method.

In Fig. S6, we plot the charge response function for $U/t_h = 2$ and 6. We will see in the next subsection that $K^{00}(\mathbf{q}, \omega)$ is related to $K^{\parallel}(\mathbf{q}, \omega)$ due to the symmetry constraint. Compared with $K^{\parallel}(\mathbf{q}, \omega)$, the contribution of the low-energy sidebands is enhanced in $K^{00}(\mathbf{q}, \omega)$, which can also be understood from the symmetry constraint [Eq. (S79)]. In the low-momentum limit, the charge response function vanishes,

$$\lim_{\mathbf{q} \rightarrow 0} K^{00}(\mathbf{q}, \omega) = 0, \quad (\text{S73})$$

since $H(\mathbf{Q} \pm \mathbf{q}) = 0$ for $\mathbf{q} \rightarrow 0$ and $\mathbf{r} = 0$.

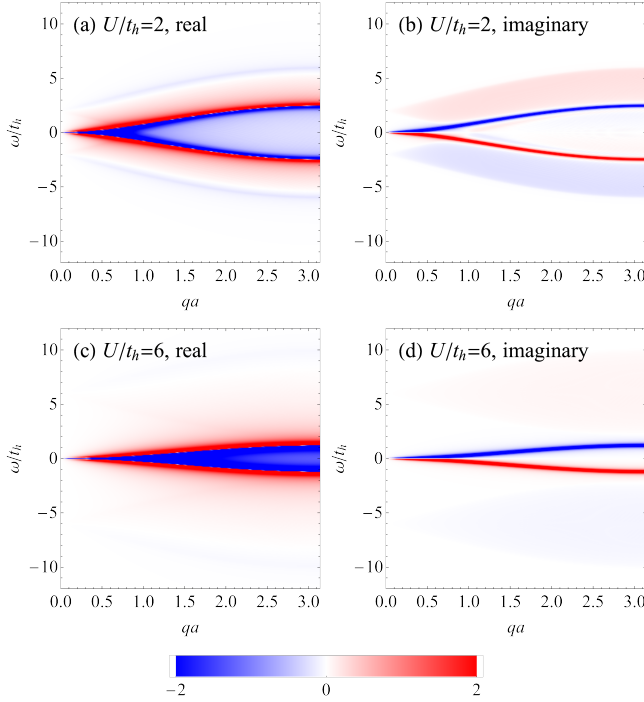


FIG. S6. Charge response function $K^{00}(\mathbf{q}, \omega)$ for the η -pairing states in the Hubbard model in units of $4c^2 e^2 t_h C_{M,N}$. (a), (b): Real (a) and imaginary (b) parts of $K^{00}(\mathbf{q}, \omega)$ for $U/t_h = 2$. (c), (d): Real (c) and imaginary (d) parts of $K^{00}(\mathbf{q}, \omega)$ for $U/t_h = 6$.

B. Symmetry constraint

Here we see how the symmetry puts a constraint on the electromagnetic response functions [37]. Our starting point is the continuity equation,

$$\frac{d}{dt}\rho(\mathbf{R}_j, t) = - \sum_{\mu=x,y,z} (J^\mu(\mathbf{R}_j) - J^\mu(\mathbf{R}_j - \mathbf{e}_\mu)), \quad (\text{S74})$$

which is a direct consequence of the U(1) symmetry of the Hubbard model. After Fourier transformation, the relation becomes

$$-i\omega\rho(\mathbf{q}, \omega) = - \sum_{\mu=x,y,z} (e^{\frac{i}{2}\mathbf{q}\cdot\mathbf{e}_\mu} - e^{-\frac{i}{2}\mathbf{q}\cdot\mathbf{e}_\mu})J^\mu(\mathbf{q}, \omega). \quad (\text{S75})$$

Taking the expectation value with respect to $|\psi_N\rangle$ and substituting the electromagnetic response function (S62) in Eq. (S75), we obtain

$$\begin{aligned} & -i\frac{\omega}{c} \sum_{\nu=0,x,y,z} K^{0\nu}(\mathbf{q}, \omega) A_\nu(\mathbf{q}, \omega) \\ &= - \sum_{\mu=x,y,z} (e^{\frac{i}{2}\mathbf{q}\cdot\mathbf{e}_\mu} - e^{-\frac{i}{2}\mathbf{q}\cdot\mathbf{e}_\mu}) \sum_{\nu=0,x,y,z} K^{\mu\nu}(\mathbf{q}, \omega) A_\nu(\mathbf{q}, \omega). \end{aligned} \quad (\text{S76})$$

Since the above relation must hold for arbitrary $A_\nu(\mathbf{q}, \omega)$, we conclude that

$$i\frac{\omega}{c} K^{0\nu}(\mathbf{q}, \omega) - \sum_{\mu=x,y,z} (e^{\frac{i}{2}\mathbf{q}\cdot\mathbf{e}_\mu} - e^{-\frac{i}{2}\mathbf{q}\cdot\mathbf{e}_\mu}) K^{\mu\nu}(\mathbf{q}, \omega) = 0. \quad (\text{S77})$$

We assume $\mathbf{q} \parallel \mathbf{e}_z$ without loss of generality. Then the relation becomes

$$K^{0\nu}(\mathbf{q}, \omega) = \frac{2c \sin \frac{q}{2}}{\omega} K^{z\nu}(\mathbf{q}, \omega). \quad (\text{S78})$$

Due to Onsager's reciprocity relation, we also have $K^{\mu\nu}(\mathbf{q}, \omega) = K^{\nu\mu}(\mathbf{q}, \omega)$. Therefore, $K^{00}(\mathbf{q}, \omega)$ and $K^{\parallel}(\mathbf{q}, \omega)$ are related to each other through

$$K^{00}(\mathbf{q}, \omega) = \frac{4c^2 \sin^2 \frac{q}{2}}{\omega^2} K^{\parallel}(\mathbf{q}, \omega). \quad (\text{S79})$$

To summarize, all the components of the electromagnetic response function $K^{\mu\nu}(\mathbf{q}, \omega)$ can be expressed in terms of $K^{\perp}(\mathbf{q}, \omega)$ and $K^{\parallel}(\mathbf{q}, \omega)$ as

$$K^{\mu\nu}(\mathbf{q}, \omega) = \begin{pmatrix} \frac{4c^2 \sin^2 \frac{q}{2}}{\omega^2} K^{\parallel}(\mathbf{q}, \omega) & 0 & 0 & \frac{2c \sin \frac{q}{2}}{\omega} K^{\parallel}(\mathbf{q}, \omega) \\ 0 & K^{\perp}(\mathbf{q}, \omega) & 0 & 0 \\ 0 & 0 & K^{\perp}(\mathbf{q}, \omega) & 0 \\ \frac{2c \sin \frac{q}{2}}{\omega} K^{\parallel}(\mathbf{q}, \omega) & 0 & 0 & K^{\parallel}(\mathbf{q}, \omega) \end{pmatrix}. \quad (\text{S80})$$

One can check that the symmetry constraint (S78) is consistent with gauge invariance in the Hubbard model.

III. DYNAMICAL ELECTROMAGNETIC FIELDS

In this section, we give a detailed description of dynamical electromagnetic fields coupled to the η -pairing states. We start with the Maxwell equations,

$$\nabla \cdot \mathbf{E} = \frac{1}{\varepsilon_0} \rho, \quad (\text{S81})$$

$$\nabla \times \mathbf{E} + \frac{\partial}{\partial t} \mathbf{B} = 0, \quad (\text{S82})$$

$$\nabla \cdot \mathbf{B} = 0, \quad (\text{S83})$$

$$\nabla \times \mathbf{B} - \frac{1}{c^2} \frac{\partial}{\partial t} \mathbf{E} = \mu_0 \mathbf{j}, \quad (\text{S84})$$

where \mathbf{E} and \mathbf{B} are electric and magnetic fields, and ρ and \mathbf{j} are the charge density and current, respectively. As usual, we introduce the scalar potential ϕ and the vector potential \mathbf{A} through

$$\mathbf{E} = -\nabla\phi - \frac{\partial}{\partial t} \mathbf{A}, \quad (\text{S85})$$

$$\mathbf{B} = \nabla \times \mathbf{A}. \quad (\text{S86})$$

In the following, we adopt the Lorenz gauge:

$$\frac{1}{c^2} \frac{\partial}{\partial t} \phi + \nabla \cdot \mathbf{A} = 0. \quad (\text{S87})$$

Then, the equations for ϕ and \mathbf{A} become

$$\frac{1}{c^2} \frac{\partial^2}{\partial t^2} \phi - \nabla^2 \phi = \frac{1}{\varepsilon_0} \rho, \quad (\text{S88})$$

$$\frac{1}{c^2} \frac{\partial^2}{\partial t^2} \mathbf{A} - \nabla^2 \mathbf{A} = \mu_0 \mathbf{j}. \quad (\text{S89})$$

To solve these equations, we assume plane-wave solutions,

$$\phi(\mathbf{r}, t) = \phi_0 e^{-i\omega t + i\mathbf{q} \cdot \mathbf{r}}, \quad (\text{S90})$$

$$\mathbf{A}(\mathbf{r}, t) = \mathbf{A}_0 e^{-i\omega t + i\mathbf{q} \cdot \mathbf{r}}, \quad (\text{S91})$$

with frequency ω and momentum \mathbf{q} . Without loss of generality, we assume $\mathbf{q} \parallel \mathbf{e}_z$. Combining the linear-response relation $j^\mu(\mathbf{q}, \omega) = -K^{\mu\nu}(\mathbf{q}, \omega) A_\nu(\mathbf{q}, \omega)$ and the gauge condition (S87), we obtain

$$-\frac{\omega^2}{c^2} \phi + q^2 \phi = \frac{1}{\varepsilon_0} K^{00}(\mathbf{q}, \omega) \frac{\phi}{c} - \frac{1}{\varepsilon_0} K^{0z}(\mathbf{q}, \omega) A_z, \quad (\text{S92})$$

$$-\frac{\omega^2}{c^2} A^x + q^2 A^x = -\mu_0 K^{xx}(\mathbf{q}, \omega) A_x, \quad (\text{S93})$$

$$-\frac{\omega^2}{c^2} A^y + q^2 A^y = -\mu_0 K^{yy}(\mathbf{q}, \omega) A_y, \quad (\text{S94})$$

$$-\frac{\omega^2}{c^2} A^z + q^2 A^z = -\mu_0 K^{zz}(\mathbf{q}, \omega) A_z + \mu_0 K^{z0}(\mathbf{q}, \omega) \frac{\phi}{c}, \quad (\text{S95})$$

$$\frac{\omega}{c^2} \phi - q A^z = 0. \quad (\text{S96})$$

Note that we use the metric $\eta^{\mu\nu} = \text{diag}(-, +, +, +)$ to write down the above equations. One can see that the transverse (A^x, A^y) and longitudinal (A^z) components are decoupled.

In the low-energy and long-wavelength limit, the above field equation can be derived from an effective Lagrangian density

$$\mathcal{L}_{\text{eff}} = -\frac{1}{4\mu_0} F_{\mu\nu} F^{\mu\nu} - V_{\text{eff}}(A^\mu) \quad (\text{S97})$$

with an effective potential

$$V_{\text{eff}}(A^\mu) = \frac{1}{2\mu_0} m^2 c^2 A_\mu A^\mu, \quad (\text{S98})$$

where $F_{\mu\nu} = \partial_\mu A_\nu - \partial_\nu A_\mu$ is the field strength, and m is the effective mass of the electromagnetic field corresponding to

$$m^2 = \frac{\mu_0}{c^2} \lim_{q \rightarrow 0} \lim_{\omega \rightarrow 0} K^\perp(\mathbf{q}, \omega) = \frac{\mu_0}{\pi c^2} D_s. \quad (\text{S99})$$

Thus, the squared mass of the electromagnetic field is proportional to the Meissner weight. In ordinary situations ($D_s > 0$), the electromagnetic field acquires a positive squared mass due to the Anderson-Higgs mechanism. In the opposite case ($D_s < 0$), the electromagnetic field becomes “tachyonic” with a negative squared mass.

A. Transverse mode

In order for the transverse modes to exist ($A^x, A^y \neq 0$), the dispersion must satisfy

$$q^2 - \frac{\omega^2}{c^2} = -\mu_0 K^\perp(\mathbf{q}, \omega), \quad (\text{S100})$$

which corresponds to Eq. (6) in the main text. While the condition (S100) gives a complicated nonlinear relation between ω and q , the situation becomes simplified at low momentum.

In the case of $U > 0$, Eq. (S100) reduces to

$$-\frac{\omega^2}{c^2} = -8\mu_0 e^2 t_h^2 C_{M,N} \left(\frac{1}{\omega + U} - \frac{1}{\omega - U} \right) \quad (\text{S101})$$

in the limit of $q \rightarrow 0$ [see Eq. (S61)]. The solution for ω^2 is given by

$$\omega^2 = \frac{1}{2} \left(U^2 \pm \sqrt{U^4 - 64\mu_0 c^2 e^2 t_h^2 C_{M,N} U} \right). \quad (\text{S102})$$

In order for ω to take a real value, the interaction strength U must satisfy

$$U^3 \geq 64\mu_0 c^2 e^2 t_h^2 C_{M,N}, \quad (\text{S103})$$

which is exactly the condition derived in the main text. In the thermodynamic limit ($M, N \rightarrow \infty$ with N/M being fixed), $C_{M,N}$ approaches $\rho(1 - \rho)$, where $\rho := (N/2)/M$ is the doublon density. In this limit, the condition (S103) becomes

$$\frac{U}{t_h} \geq 4 \left(\frac{\mu_0 c^2 e^2 \rho(1 - \rho)}{t_h} \right)^{\frac{1}{3}}. \quad (\text{S104})$$

In Fig. S7, we plot the parameter space where the frequency ω has an imaginary part. One can see that a wide range of the parameter region shows a dynamical instability of the electromagnetic field coupled to the η -pairing state in the long-wavelength limit. The real part of the frequency at $q \rightarrow 0$ is given by

$$\text{Re } \omega = \frac{1}{2} \sqrt{\sqrt{64\mu_0 c^2 e^2 t_h^2 C_{M,N} U} + U^2}, \quad (\text{S105})$$

which is proportional to $U^{1/4}$ at small U . The imaginary part of the frequency at $q \rightarrow 0$ is given by

$$\text{Im } \omega = \frac{1}{2} \sqrt{\sqrt{64\mu_0 c^2 e^2 t_h^2 C_{M,N} U} - U^2} \quad (\text{S106})$$

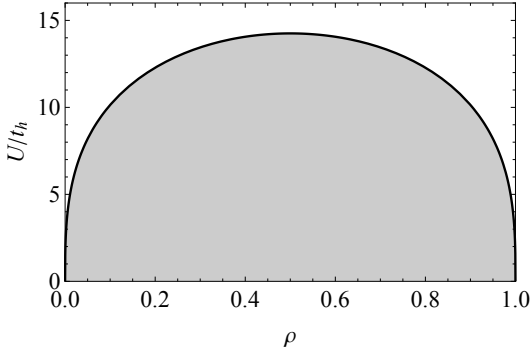


FIG. S7. Parameter space (shaded region) where the transverse electromagnetic field coupled to the η -pairing state in the Hubbard model becomes unstable in the long-wavelength limit ($\mathbf{q} \rightarrow 0$).

for $U^3 < 64\mu_0 c^2 e^2 t_h^2 C_{M,N}$.

More generally, if we take into account arbitrary \mathbf{q} modes, we can prove that a dynamical instability exists for all U and ρ . First, we observe that $K^\perp(\mathbf{q}, \omega)$ in Eq. (S31) takes a real value if and only if $|\omega + U| > 4t_h \sin \frac{q}{2}$ and $|\omega - U| > 4t_h \sin \frac{q}{2}$. Let us first consider the case of $0 < \omega < U - 4t_h \sin \frac{q}{2}$. Using the result for $K^\perp(\mathbf{q}, \omega)$ in Eq. (S31), the dispersion relation (S100) can be written as

$$q^2 - \frac{\omega^2}{c^2} = -8\mu_0 e^2 t_h^2 C_{M,N} \left\{ \frac{1}{\sqrt{(\omega + U)^2 - 16t_h^2 \sin^2 \frac{q}{2}}} + \frac{1}{\sqrt{(\omega - U)^2 - 16t_h^2 \sin^2 \frac{q}{2}}} \right\}, \quad (\text{S107})$$

which is negative definite. Therefore, we have $\omega > cq$. For the other case of $\omega > U + 4t_h \sin \frac{q}{2}$, the condition (S100) reads

$$q^2 - \frac{\omega^2}{c^2} = -8\mu_0 e^2 t_h^2 C_{M,N} \left\{ \frac{1}{\sqrt{(\omega + U)^2 - 16t_h^2 \sin^2 \frac{q}{2}}} - \frac{1}{\sqrt{(\omega - U)^2 - 16t_h^2 \sin^2 \frac{q}{2}}} \right\}, \quad (\text{S108})$$

which is positive definite since $(\omega + U)^2 - 16t_h^2 \sin^2 \frac{q}{2} > (\omega - U)^2 - 16t_h^2 \sin^2 \frac{q}{2}$. Therefore, we have $\omega < cq$.

In Fig. S8, we plot the range of (q, ω) in which the real solution for Eq. (S100) is allowed. Since the allowed region is separated into two disjoint islands, it is clear from a topological point of view that the real band dispersion $\omega = \omega(q)$ for all q is not possible. This means that there must always be a region in (q, ω) where the solution for Eq. (S100) becomes complex. Thus, there is a dynamical instability for arbitrary $U(> 0)$ and ρ .

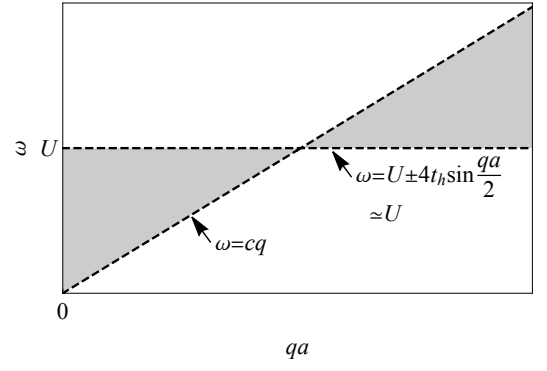


FIG. S8. Schematic illustration of the range of (q, ω) in which the real solution for Eq. (S100) with $U > 0$ is allowed as shown by the shaded region for $qa \ll 1$. The dashed lines indicate that the boundary is not included.

In the attractive case ($U < 0$), the mode equation in the long-wavelength limit is similarly given by Eq. (S101). The solution for ω^2 is the same as Eq. (S102). When $U < 0$, ω^2 is always real. However, there exists a solution with $\omega^2 < 0$ when one chooses the minus sign in Eq. (S102). Hence the frequency becomes imaginary for $\mathbf{q} \rightarrow 0$. The inverse of the imaginary part of ω is given by

$$\frac{1}{\text{Im } \omega} = \frac{1}{\sqrt{\frac{1}{2} \left(\sqrt{U^4 - 64\mu_0 c^2 e^2 t_h^2 C_{M,N} U} - U^2 \right)}}. \quad (\text{S109})$$

In the attractive case, the electromagnetic field is dynamically unstable against the $\mathbf{q} = 0$ mode. This corresponds to the fact that the electromagnetic field has a negative squared mass. Physically, the electromagnetic field with a long wavelength penetrates deeply inside the η pairing state, transferring the kinetic energy of doublons to the electromagnetic field. The time scale of the growth of this instability is determined by Eq. (S109).

Combining the arguments for the two cases ($U > 0$ and $U < 0$), we have established that the electromagnetic field coupled to the η -pairing state is always dynamically unstable for all U and ρ .

B. Longitudinal mode

The mode equation for the longitudinal components can be derived from Eqs. (S92), (S95), and (S96). To simplify the situation, we focus on the low-momentum region ($qa \ll 1$). In this region, the dispersion is determined by

$$q^2 - \frac{\omega^2}{c^2} = -\mu_0 K^\parallel(q, \omega) \left(1 - \frac{c^2 q^2}{\omega^2} \right), \quad (\text{S110})$$

where we have used the relation (S80). In the limit of $q \rightarrow 0$, the mode equation becomes

$$-\frac{\omega^2}{c^2} = -\mu_0 \lim_{q \rightarrow 0} K^{\parallel}(q, \omega). \quad (\text{S111})$$

If we recall the relation (S61), the dispersion (S111) is the same as that of the transverse mode (S100). Therefore, the longitudinal mode has the same dynamical instability as the transverse one at low momentum.

IV. MAGNETIC PROPERTIES OF TACHYONIC SUPERCONDUCTORS

In this section, we describe static magnetic properties of tachyonic superconductors realized as the η -pairing states in the Hubbard model with $U < 0$. As shown in the main text and in the preceding section, the tachyonic superconductors are dynamically unstable. Here we focus on the response of the η -pairing states against static magnetic fields within the linear-response regime, and do not consider their decay dynamics.

The static magnetic field \mathbf{B} obeys the following Maxwell equations:

$$\nabla \cdot \mathbf{B} = 0, \quad (\text{S112})$$

$$\nabla \times \mathbf{B} = \mu_0 \mathbf{j}. \quad (\text{S113})$$

We introduce a static vector potential \mathbf{A} as $\mathbf{B} = \nabla \times \mathbf{A}$. If we take the Coulomb gauge ($\nabla \cdot \mathbf{A} = 0$), the equation for \mathbf{A} becomes

$$\nabla^2 \mathbf{A} = -\mu_0 \mathbf{j}. \quad (\text{S114})$$

To solve the equation, we assume a plane-wave form,

$$\mathbf{A}(\mathbf{r}) = \mathbf{A}_0 e^{i\mathbf{q} \cdot \mathbf{r}}, \quad (\text{S115})$$

with amplitude \mathbf{A}_0 and wave number \mathbf{q} . Without loss of generality, we choose $\mathbf{q} = q\mathbf{e}_z$. We apply the linear-response theory to the η -pairing states to obtain the equations for \mathbf{A}_0 :

$$\mathbf{q} \cdot \mathbf{A}_0 = 0, \quad (\text{S116})$$

$$\begin{aligned} -q^2 A_0^\mu &= -\mu_0 j^\mu(\mathbf{q}) \\ &= \mu_0 \sum_\nu K^{\mu\nu}(\mathbf{q}, \omega=0) A_{0\nu} \quad (\mu, \nu = x, y, z). \end{aligned} \quad (\text{S117})$$

From Eq. (S116), we find $A_0^z = 0$. In order for the solution $A_0^\mu \neq 0$ to exist, q must satisfy a nonlinear equation,

$$\begin{aligned} q^2 &= -\mu_0 K^\perp(\mathbf{q}, \omega=0) \\ &= -16\mu_0 e^2 t_h^2 C_{M,N} \\ &\times \begin{cases} \frac{\text{sgn}(U)}{\sqrt{U^2 - 16t_h^2 \sin^2 \frac{q}{2}}} & \text{for } |U| > 4t_h \sin \frac{q}{2}; \\ 0 & \text{for } |U| < 4t_h \sin \frac{q}{2}, \end{cases} \end{aligned} \quad (\text{S118})$$

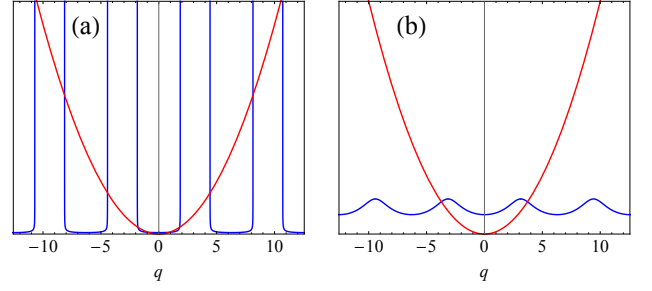


FIG. S9. Graphical illustration of Eq. (S118) for (a) $-4t_h < U < 0$ and (b) $U < -4t_h$. The left-hand side of Eq. (S118) is shown by the red curve, while the right-hand side is shown by the blue curve.

# of real solutions for Eq. (S118)	
$U > 0$	0
$-4t_h < U < 0$	∞
$U < -4t_h$	2

TABLE I. List of the number of real solutions for Eq. (S118) with $16\mu_0 e^2 t_h a / \hbar^2 \ll 1$.

where we have used the result (S31).

One can immediately see that a real solution for Eq. (S118) does not exist for $U > 0$. This is nothing but the Meissner effect; that is, a magnetic field cannot propagate freely into superconductors. In fact, the magnetic field decays exponentially in space with the penetration depth

$$\lambda = \sqrt{\frac{U}{16\mu_0 e^2 t_h^2 C_{M,N}}}. \quad (\text{S119})$$

On the other hand, when $U < 0$ a real solution is possible as is clear from the graphical illustration of Eq. (S118) in Fig. S9. Thus, a magnetic field *can* penetrate into tachyonic superconductors without decay.

From Fig. S9, we can see that the number of real solutions for Eq. (S118) changes at the boundary of $U = -4t_h$. In Table. I, we list the number of real solutions for Eq. (S118). This result suggests that the number of modes of magnetic fields that can propagate inside tachyonic superconductors for $-4t_h < U < 0$ is different from that for $U < -4t_h$. Following the main text, we call the former a type-I tachyonic superconductor, and the latter a type-II tachyonic superconductor.

In the case of the type-I tachyonic superconductor, we further classify the solutions into two types according to the number of real solutions in the range of $-\pi < q < \pi$. When U belongs to the range $(-4t_h <) U_* < U < 0$ with a certain boundary U_* , real solutions for Eq. (S118) do not exist in $-\pi < q < \pi$. Since $16\mu_0 e^2 t_h a / \hbar^2 \ll 1$ for ordinary materials ($t_h \sim 1[\text{eV}]$ and $a \sim 1[\text{\AA}]$), the

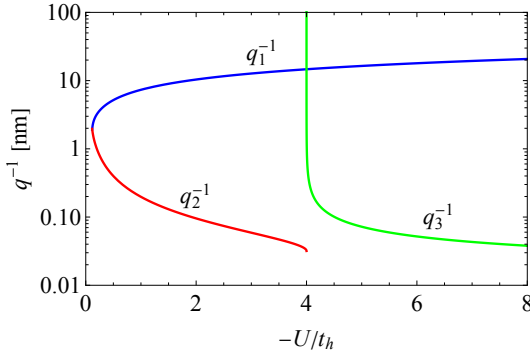


FIG. S10. Log plot of q_1^{-1} , q_2^{-1} , and q_3^{-1} for $t_h = 1[\text{eV}]$, $a = 1[\text{\AA}]$, and $\rho = 0.5$ as a function of $-U/t_h$.

threshold U_* is approximately given as

$$\frac{U_*}{t_h} \approx -2\sqrt{3}(4\mu_0 e^2 t_h C_{M,N})^{\frac{1}{3}}. \quad (\text{S120})$$

For $-4t_h < U < U_*$, there exist four real solutions in $-\pi < q < \pi$, which are denoted by $\pm q_1$ and $\pm q_2$ with $0 < q_1 < q_2$. Using $16\mu_0 e^2 t_h a / \hbar^2 \ll 1$ again, we can approximately evaluate q_1 and q_2 as

$$q_1 \approx \sqrt{\frac{16\mu_0 e^2 t_h^2 C_{M,N}}{-U}}, \quad (\text{S121})$$

$$q_2 \approx 2 \sin^{-1} \left(\frac{-U}{4t_h} \right). \quad (\text{S122})$$

Note that q_1 corresponds to the inverse of the analytically continued London's penetration depth ($q_1 = |\lambda|^{-1}$). If we extend the range of q to $-\infty < q < \infty$, there are infinitely many real solutions. They are approximately given as $\pm q_1$ and $\pm q_2 + 2n\pi$ ($n \in \mathbb{Z}$).

In the case of the type-II tachyonic superconductor, there are only two real solutions $\pm q_1$ approximately given by (S121). Instead, there emerge infinitely many complex solutions approximately given by $\pm i q_3 + 2n\pi$ ($n \in \mathbb{Z}$) with

$$q_3 \approx 2 \cosh^{-1} \left(\frac{-U}{4t_h} \right). \quad (\text{S123})$$

Physically, these solutions correspond to a magnetic field localized near the surface of a tachyonic superconductor. The localization length q_3^{-1} diverges at $U = U'_c = -4t_h$ as $q_3^{-1} \sim |U - U'_c|^{-1/2}$.

In Fig. S10, we plot q_1^{-1} , q_2^{-1} , and q_3^{-1} for typical parameters. The q_1 mode produces a long-period magnetic structure with the period of the order of $|\lambda| \gg a$. On the other hand, the q_2 mode provides a short-period magnetic structure with the period length of the order of the lattice constant a . In type-I tachyonic superconductors, both the long- and short-period structures are allowed to exist, whereas in type-II tachyonic superconductors the short-period magnetic structure is screened, and it can penetrate only near the surface.

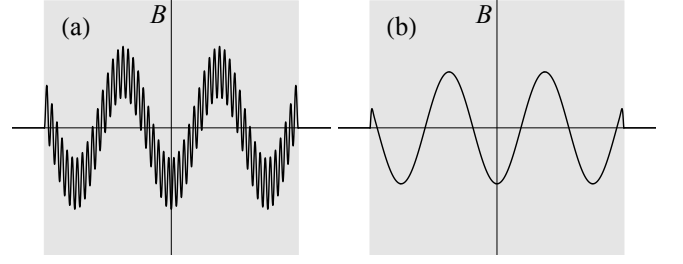


FIG. S11. Examples of static magnetic fields $B = B(x)$ that can exist inside (a) type-I and (b) type-II tachyonic superconductors shown by shaded regions.

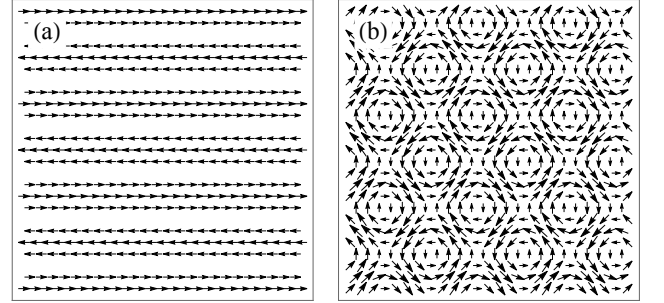


FIG. S12. Examples of (a) stripe-like and (b) vortex-antivortex-like magnetic structures in tachyonic superconductors shown in a two-dimensional plane.

In Fig. S11, we show examples of magnetic fields that can be realized in type-I [Fig. S11(a)] and type-II (b) tachyonic superconductors. Even when there is no magnetic field outside of tachyonic superconductors, nonzero magnetic fields can be trapped statically inside tachyonic superconductors. To support those magnetic fields, constant electric currents are flowing in the bulk of tachyonic superconductors. In the type-II tachyonic superconductor, there is also a surface current to satisfy the boundary condition.

Various q modes can be linearly superposed in several different directions. In Fig. S12, we show two examples of magnetic structures that can be realized in tachyonic superconductors. If one only takes a single q_1 mode, it gives a stripe-like structure as shown in Fig. S12(a). Here we neglect short-period structures (q_2 modes). If one superposes two q_1 modes in x and y directions, one obtains a square lattice with alternating vortex and antivortex structures as shown in Fig. S12. This is to be contrasted with Abrikosov's triangular lattice of vortices in type-II superconductors. One can also superimpose three q_1 modes in three different directions, creating a three-dimensional magnetic structure (not shown). In this way, various configurations of magnetic fields can be trapped in tachyonic superconductors. We note, however, that these structures are not dynamically stable as shown in the main text and in the preceding section.

V. SPONTANEOUS LIGHT EMISSION

In this section, we evaluate the rate of spontaneous light emission for η -pairing states in the Hubbard model with $U > 0$. In the repulsive case, doublons can decay spontaneously into pairs of single particles by emitting light with frequency $\omega = U$. After emitting light, the η -pairing state $|\psi_N\rangle$ is transformed into

$$J^\mu(\mathbf{q} = 0)|\psi_N\rangle = \frac{e}{\sqrt{\mathcal{N}_N}} N(\eta^+)^{\frac{N}{2}-1} \sum_{\mathbf{k}} v^\mu(\mathbf{k}) c_{\mathbf{k}\uparrow}^\dagger c_{\mathbf{Q}-\mathbf{k}\downarrow}^\dagger |0\rangle, \quad (\text{S124})$$

where $v^\mu(\mathbf{k}) = \frac{\partial \varepsilon_{\mathbf{k}}}{\partial k^\mu} = 2t_h \sin k^\mu$ is the group velocity ($\varepsilon_{\mathbf{k}} = -2t_h \sum_{\mu=x,y,z} \cos k^\mu$ is the band dispersion).

Let us define a one-doublon-broken state [16]

$$|\zeta_{N,\mathbf{a}}\rangle = \frac{1}{\sqrt{\mathcal{N}_{N,\mathbf{a}}}} (\eta^+)^{\frac{N}{2}-1} \eta_{\mathbf{a}}^+ |0\rangle, \quad (\text{S125})$$

where $\mathcal{N}_{N,\mathbf{a}}$ is the normalization constant (such that $\langle \zeta_{N,\mathbf{a}} | \zeta_{N,\mathbf{a}'} \rangle = \delta_{\mathbf{a},\mathbf{a}'}$), \mathbf{a} represents a lattice-site coordinate, and

$$\eta_{\mathbf{a}}^+ = \sum_{\mathbf{k}} e^{-i\mathbf{k}\cdot\mathbf{a}} c_{\mathbf{k}\uparrow}^\dagger c_{\mathbf{Q}-\mathbf{k}\downarrow}^\dagger. \quad (\text{S126})$$

The state $|\zeta_{N,\mathbf{a}}\rangle$ consists of $\frac{N}{2} - 1$ doublons with momentum \mathbf{Q} and two unpaired particles with the lattice spacing \mathbf{a} . One can show that $|\zeta_{N,\mathbf{a}}\rangle$ with $\mathbf{a} \neq 0$ is an exact eigenstate of the Hubbard model [Eq. (1) in the main text] with the eigenenergy $-U$. At $\mathbf{a} = 0$, we have $|\zeta_{N,\mathbf{a}}\rangle = |\psi_N\rangle$. Using $|\zeta_{N,\mathbf{a}}\rangle$, we can write the one-photon emitted state (S124) as

$$J^\mu(\mathbf{q} = 0)|\psi_N\rangle = e \sqrt{\frac{\mathcal{N}_{N,\mathbf{a}}}{\mathcal{N}_N}} \frac{N}{M} \sum_{\mathbf{k}} v^\mu(\mathbf{k}) \sum_{\mathbf{a} \neq 0} e^{i\mathbf{k}\cdot\mathbf{a}} |\zeta_{N,\mathbf{a}}\rangle. \quad (\text{S127})$$

Therefore, all the states that are accessible by one-photon emission are covered by the eigenstates $|\zeta_{N,\mathbf{a}}\rangle$ ($\mathbf{a} \neq 0$).

The rate of spontaneous emission is given by Einstein's A coefficient [50]:

$$\Gamma = \frac{\omega^3}{3\pi\epsilon_0 c^3 \hbar} \sum_{\mu} |\langle e | P^\mu | \sigma \rangle|^2, \quad (\text{S128})$$

where P^μ is the polarization operator, $|\sigma\rangle$ is an initial state, and $|e\rangle$ is a one-photon emitted state. In the present case, we take $|\sigma\rangle = |\psi_N\rangle$ and $|e\rangle = |\zeta_{N,\mathbf{a}}\rangle$. Since $\frac{d}{dt} P^\mu = J^\mu$, the rate Γ is rewritten as

$$\begin{aligned} \Gamma &= \frac{\omega}{3\pi\epsilon_0 c^3 \hbar} \sum_{\mu} \sum_{\mathbf{a}} |\langle \zeta_{N,\mathbf{a}} | J^\mu | \psi_N \rangle|^2 \\ &= \frac{e^2 \omega}{3\pi\epsilon_0 c^3 \hbar} \sum_{\mu} \sum_{\mathbf{a}} \frac{\mathcal{N}_{N,\mathbf{a}}}{\mathcal{N}_N} \frac{N^2}{M^2} \left| \sum_{\mathbf{k}} v^\mu(\mathbf{k}) e^{i\mathbf{k}\cdot\mathbf{a}} \right|^2. \end{aligned} \quad (\text{S129})$$

Using Eq. (S13) and

$$\mathcal{N}_{N,\mathbf{a}} = \frac{M(M-2)!(\frac{N}{2}-1)!}{(M-\frac{N}{2}-1)!} \quad (\mathbf{a} \neq 0), \quad (\text{S130})$$

we obtain

$$\Gamma = \frac{8e^2 \omega t_h^2 a^2 d C_{M,N}}{3\pi\epsilon_0 c^3 \hbar^3} M, \quad (\text{S131})$$

where d is the dimension of the system. One can see that the rate Γ is proportional to the system size, which is natural because the doublon decay can take place at any lattice site with equal probability.

For ordinary three-dimensional materials, we substitute $t_h = 1$ [eV], $\omega = U = 1$ [eV], $a = 1$ [Å], $\rho = 0.5$, and $d = 3$ in Eq. (S131), obtaining

$$\frac{\Gamma}{M} = 2.3 \times 10^7 \text{ [s}^{-1}\text{]}. \quad (\text{S132})$$